Dynamic analysis of layered systems under a moving harmonic rectangular load based on the spectral element method

Sun, Zhaojie; Kasbergen, Cor; Skarpas, Athanasios; Anupam, Kumar; van Dalen, Karel N.; Erkens, Sandra M.J.G.

DOI
10.1016/j.ijsolstr.2019.06.022

Publication date
2019

Document Version
Accepted author manuscript

Published in
International Journal of Solids and Structures

Dynamic analysis of layered systems under a moving harmonic rectangular load based on the spectral element method

Zhaojie Sun[a,*], Cor Kasbergen[a], Athanasios Skarpas[b,a], Kumar Anupam[a], Karel N. van Dalen[a], Sandra M.J.G. Erkens[a]

a. Department of Engineering Structures, Faculty of Civil Engineering and Geosciences, Delft University of Technology, Stevinweg 1, 2628 CN, Delft, the Netherlands

b. Department of Civil Infrastructure and Environmental Engineering, College of Engineering, Khalifa University, P.O. Box 127788, Abu Dhabi, United Arab Emirates

Abstract: In order to design high-performance roadways, a robust tool which can compute the structural response caused by moving vehicles is necessary. Therefore, this paper proposes a spectral element method-based model to accurately and effectively predict the 3D dynamic response of layered systems under a moving load. A layer spectral element and a semi-infinite spectral element are developed to respectively model a layer and a half-space, and the combinations of these two elements can simulate layered systems. The detailed mathematical derivation and numerical validation of the proposed model are included. Addition- ally, this model is used to investigate the dynamic characteristics of a pavement structure under a moving harmonic rectangular load. The results show that the proposed model can accurately predict the dynamic response of layered systems caused by a moving load. It is also found that the vertical displacement amplitude curves of surface points caused by a moving harmonic load are asymmetric along the moving direction, and this property is more dominant at higher velocities. In addition, the amplitudes of these vertical displacements are smaller if the loading frequency is higher or the loss factor is bigger. Finally, the loading area and Poisson's ratio only have effect on the displacement amplitudes of points in the close vicinity of the loading area. The proposed model is beneficial to the development of engineering methods for pavement design and is a promising parameter back-calculation engine for pavement

quality evaluation.

Keywords: Dynamic response; Layered systems; Moving load; Spectral element method; Doppler effect

1. Introduction

Roadways are important infrastructures and should be well- designed. In order to ensure the performance, a clear understanding of the response of roadways caused by moving vehicles is necessary. Theoretically, this problem can be regarded as the dynamic analysis of semi-infinite or layered media caused by a moving load, which is generally solved by using either analytical or numerical methods.

Analytical methods generally give exact solutions to dynamic problems, and these methods are usually efficient. For example, Eason (1965) investigated the stresses in a semi-infinite elastic solid caused by moving surface forces with different loading conditions using integral transforms. Vostroukhov and Metrikine (2003) proposed a theoretical model to analyse the steady-state dynamic response of a railway track caused by moving trains, through which an analytical expression of the steady-state deflection of the rails was obtained. However, the analytical solutions are generally only valid for specific structural and loading configurations, and these solutions are usually difficult to calculate because they often contain complicated integrals with singular points.

Numerical methods, such as the finite element method (FEM) and the boundary element method (BEM), are powerful tools for the dynamic analysis of solid media with different structural combinations and loading conditions. For instance, Zaghloul and White (1993) developed a three-dimensional dynamic finite element program to analyse the behaviour of flexible pavements caused by loads moving at different velocities. Andersen and Nielsen (2003) conducted boundary element analysis of the steady-state response of an elastic half-space caused by a surface moving load. However, numerical methods are usually time and resource intensive, and numerical distortions may occur in some cases.

The limitations of analytical and numerical methods may hinder their application in engineering, especially for the dynamic analysis of layered systems. Hence, a semi-analytical method called the spectral element method (SEM) (Doyle, 1997; Al-Khoury et al., 2002; Lee, 2009) is used in this paper to analyse the 3D dynamic response of layered systems caused by a moving load. The SEM is promising for efficient dynamic analysis because it has the advantages of both spectral analysis and finite element method. In the SEM, one element is sufficient to represent a whole layer because of the exact description of mass distribution, which reduces the size of

the system of dynamic equations and further increases the computational efficiency. Moreover, this method discretises the continuous integrals into series summations, which is more convenient for numerical calculation. The SEM has been successfully used for analysing the 2D dynamic response of layered systems. For example, You et al. (2018) investigated dynamic response of transversely isotropic pavement structure under axisymmetric impact load in cylindrical coordinate system based on the SEM. Yan et al. (2018) applied the SEM to predict the dynamic response of a 2D layered system subject to a moving harmonic strip load. However, the SEM has rarely been applied for the 3D dynamic analysis of layered systems under a moving harmonic rectangular load, which is the main focus of this study.

This paper includes the detailed mathematical formulation of a 3D dynamic model for layered systems under a moving harmonic rectangular load based on the SEM. The accuracy of this model has been verified both numerically and experimentally. The proposed model can be used to analyse the 3D dynamic response of pavement structures caused by a moving harmonic rectangular load, which contributes to the development of engineering methods for pavement design. Furthermore, this model could be combined with proper optimisation algorithms to back-calculate the parameters of pavement structures by analysing the response, which is useful for pavement quality evaluation.

2. Model formulation

In this section, the detailed formulation of a model which can predict the 3D dynamic response of elastic layered systems subjected to a uniformly moving, harmonically varying, evenly distributed, rectangular surface load is presented. With considering the loading conditions caused by moving vehicles and structural parameters of pavement systems, this model can be used as a tool for structural design to ensure the durability.

2.1. Introduction of moving coordinate system

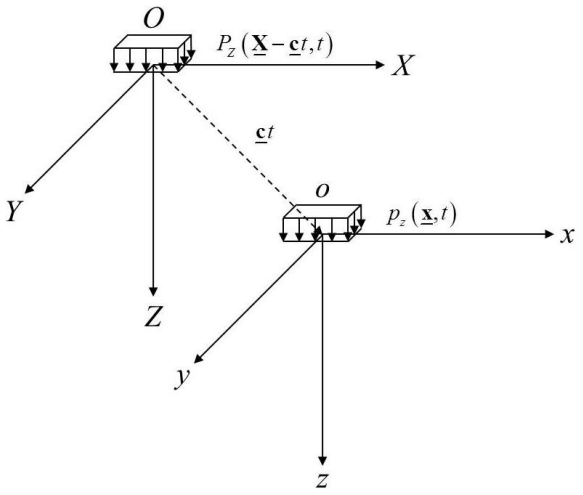

Figure 1. Schematic representation of coordinate system transformation.

As shown in Figure 1, in order to deal with the moving load problem, it is convenient to introduce a stationary Cartesian coordinate system (*OXYZ*) and a moving Cartesian coordinate system (*oxyz*) (Jones et al., 1998; Lefeuve-Mesgouez et al., 2000; Metrikine, 2004). The stationary coordinate system does not move and its origin is located at the centre of the loading area when time is zero. The moving coordinate system follows the load and its origin is located at the centre of the moving loading area. The moving velocity is assumed to be constant and is described by a vector $\underline{\mathbf{c}} = \begin{bmatrix} c_x & c_y & c_z \end{bmatrix}^{\mathrm{T}}$. The stationary coordinate vector is notated as $\underline{\mathbf{X}} = \begin{bmatrix} X & Y & Z \end{bmatrix}^{\mathrm{T}}$, and the moving coordinate vector is notated as $\underline{\mathbf{x}} = \begin{bmatrix} x & y & z \end{bmatrix}^{\mathrm{T}}$. The relationship between these two coordinate vectors can be expressed as follows:

$$\underline{\mathbf{x}} = \underline{\mathbf{X}} - \underline{\mathbf{c}}t \tag{1}$$

in which t is time. These two coordinate systems are coincident when $t = 0$.

Additionally, the partial derivatives in the two coordinate systems have the following relationships for nonnegative integer *n*:

$$\frac{\partial^n}{\partial \underline{\mathbf{X}}^n} = \frac{\partial^n}{\partial \underline{\mathbf{x}}^n} \tag{2}$$

$$\frac{\partial^n}{\partial t^n}\Big|_{\underline{\mathbf{X}}} = \left(\frac{\partial}{\partial t} - \underline{\mathbf{c}} \cdot \frac{\partial}{\partial \underline{\mathbf{x}}}\right)^n \Big|_{\underline{\mathbf{x}}} \tag{3}$$

where $\underline{\mathbf{c}} \cdot \frac{\partial}{\partial \underline{\mathbf{x}}} = c_x \frac{\partial}{\partial x} + c_y \frac{\partial}{\partial y} + c_z \frac{\partial}{\partial z}$.

2.2. Wave motion in a semi-infinite medium under a surface moving load

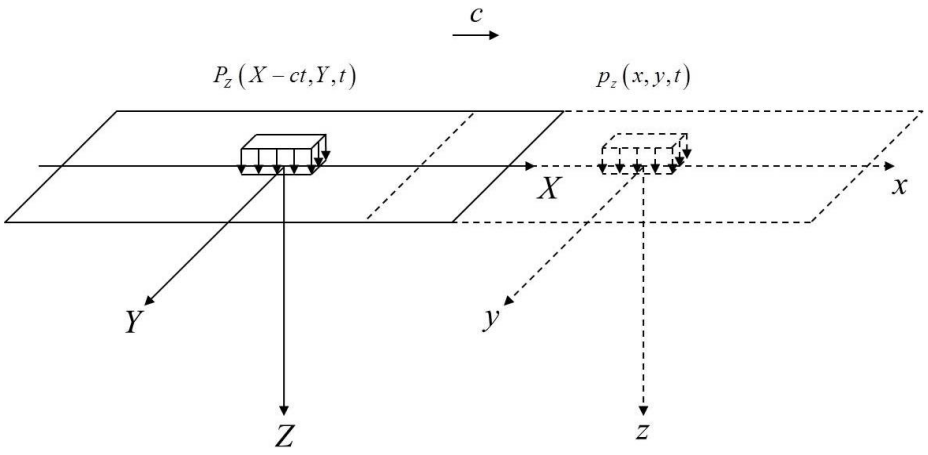

Figure 2. Schematic representation of a semi-infinite medium under a surface moving load.

As shown in Figure 2, a homogeneous, isotropic, and linear-elastic semi-infinite medium is subjected to a surface load which moves along *X*-axis with a constant speed *c*. The corresponding wave motion in this medium is considered first. In the stationary coordinate system (*OXYZ*), the equations of motion for the medium can be expressed by Navier's equation in the absence of body forces:

$$(\lambda + \mu)\nabla_0 \nabla_0 \cdot \underline{\mathbf{U}} + \mu \nabla_0^2 \underline{\mathbf{U}} = \rho \frac{\partial^2 \underline{\mathbf{U}}}{\partial t^2} \tag{4}$$

in which $\nabla_0 = \left[\frac{\partial}{\partial X} \quad \frac{\partial}{\partial Y} \quad \frac{\partial}{\partial Z} \right]^{\mathrm{T}}$ is the Del operator, $\nabla_0^2 = \frac{\partial^2}{\partial X^2} + \frac{\partial^2}{\partial Y^2} + \frac{\partial^2}{\partial Z^2}$ is the Laplacian operator, $\underline{\mathbf{U}}(\underline{\mathbf{X}}, t) = \left[U_X \quad U_Y \quad U_Z \right]^{\mathrm{T}}$ is the displacement vector, ρ is the mass density, and λ and μ are Lamé constants defined by Young's modulus E and Poisson's ratio ν.

An elegant approach to solve the Navier's equation is using the Helmholtz decomposition, which expresses a displacement field in the following form:

$$\underline{\mathbf{U}} = \nabla_0 \Phi + \nabla_0 \times \underline{\mathbf{\Psi}} \tag{5}$$

where $\Phi(\underline{\mathbf{X}}, t)$ is a scalar potential related to the P-wave, and

$\underline{\boldsymbol{\Psi}}(\underline{\mathbf{X}},t)=\begin{bmatrix}\Psi_X & \Psi_Y & \Psi_Z\end{bmatrix}^{\mathrm{T}}$ is a vector potential related to the S-wave. It can be seen that the three components of the displacement vector are related to four other functions, the scalar potential and the three components of the vector potential, which indicates that an additional constraint condition is needed (Achenbach, 1999). The additional constraint condition can have different forms (Vostroukhov and Metrikine, 2003; Hung and Yang, 2001), but the solution is uniquely determined by the governing equations and boundary conditions by virtue of the uniqueness theorem. In this paper, the Gauge condition $\nabla_0\cdot\underline{\boldsymbol{\Psi}}(\underline{\mathbf{X}},t)=0$ is taken as the additional constraint condition.

The velocity vector of the load is $\underline{\mathbf{c}}=\begin{bmatrix}c & 0 & 0\end{bmatrix}^{\mathrm{T}}$, which means movement with constant velocity c along the *x*-axis. According to the relationship between the two coordinate systems, equation (4) has the following form in the moving coordinate system:

$$(\lambda+\mu)\nabla\nabla\cdot\underline{\mathbf{u}}+\mu\nabla^2\underline{\mathbf{u}}=\rho\left(\frac{\partial}{\partial t}-c\frac{\partial}{\partial x}\right)^2\underline{\mathbf{u}} \tag{6}$$

in which $\nabla=\begin{bmatrix}\dfrac{\partial}{\partial x} & \dfrac{\partial}{\partial y} & \dfrac{\partial}{\partial z}\end{bmatrix}^{\mathrm{T}}$ is the Del operator in the moving coordinate system, $\nabla^2=\dfrac{\partial^2}{\partial x^2}+\dfrac{\partial^2}{\partial y^2}+\dfrac{\partial^2}{\partial z^2}$ is the Laplacian operator in the moving coordinate system, $\underline{\mathbf{u}}(\underline{\mathbf{x}},t)=\begin{bmatrix}u_x & u_y & u_z\end{bmatrix}^{\mathrm{T}}$ is the displacement vector in the moving coordinate system.

In the moving coordinate system, equation (5) has the following form:

$$\underline{\mathbf{u}}=\nabla\phi+\nabla\times\underline{\boldsymbol{\psi}} \tag{7}$$

where $\phi(\underline{\mathbf{x}},t)$ and $\underline{\boldsymbol{\psi}}(\underline{\mathbf{x}},t)=\begin{bmatrix}\psi_x & \psi_y & \psi_z\end{bmatrix}^{\mathrm{T}}$ are the scalar potential and the vector potential in the moving coordinate system, respectively. The Gauge condition in the moving coordinate system reads $\nabla\cdot\underline{\boldsymbol{\psi}}(\underline{\mathbf{x}},t)=0$.

By substituting equation (7) into equation (6), the following uncoupled wave

equations in the moving coordinate system are obtained (for more details see Appendix A):

$$\nabla^2\phi-\frac{1}{c_{\mathrm{P}}^2}\left(\frac{\partial}{\partial t}-c\frac{\partial}{\partial x}\right)^2\phi=0 \tag{8}$$

$$\nabla^2\underline{\boldsymbol{\psi}}-\frac{1}{c_{\mathrm{S}}^2}\left(\frac{\partial}{\partial t}-c\frac{\partial}{\partial x}\right)^2\underline{\boldsymbol{\psi}}=\underline{\mathbf{0}} \tag{9}$$

in which $c_{\mathrm{P}}=\sqrt{(\lambda+2\mu)/\rho}$ is the velocity of the P-wave, and $c_{\mathrm{S}}=\sqrt{\mu/\rho}$ is the velocity of the S-wave.

In order to solve equations (8) and (9), the following Fourier transform pair with respect to time is used:

$$\hat{q}(\underline{\mathbf{x}},\omega)=\frac{1}{2\pi}\int_{-\infty}^{\infty}q(\underline{\mathbf{x}},t)e^{-\mathrm{i}\omega t}dt \tag{10}$$

$$q(\underline{\mathbf{x}},t)=\int_{-\infty}^{\infty}\hat{q}(\underline{\mathbf{x}},\omega)e^{\mathrm{i}\omega t}d\omega \tag{11}$$

where i is the imaginary unit satisfying $\mathrm{i}^2=-1$, ω is angular frequency, $q(\underline{\mathbf{x}},t)$ is an arbitrary quantity in time domain, and $\hat{q}(\underline{\mathbf{x}},\omega)$ is the corresponding quantity in frequency domain. After applying the above Fourier transform, equations (7) to (9) become:

$$\hat{\underline{\mathbf{u}}}=\nabla\hat{\phi}+\nabla\times\hat{\underline{\boldsymbol{\psi}}} \tag{12}$$

$$\nabla^2\hat{\phi}-\frac{1}{c_{\mathrm{P}}^2}\left(\mathrm{i}\omega-c\frac{\partial}{\partial x}\right)^2\hat{\phi}=0 \tag{13}$$

$$\nabla^2\hat{\underline{\boldsymbol{\psi}}}-\frac{1}{c_{\mathrm{S}}^2}\left(\mathrm{i}\omega-c\frac{\partial}{\partial x}\right)^2\hat{\underline{\boldsymbol{\psi}}}=\underline{\mathbf{0}} \tag{14}$$

in which the "hat" means that these quantities are expressed in the frequency domain.

In the Cartesian coordinate system, the solutions of equations (13) and (14) can be retrieved in exponential forms. According to the phase matching principle (Zhao et al., 2016), different waves should have the same phase at the boundary (e.g. the

surface $z = 0$). Consequently, the P-wave and S-wave have the same wavenumbers not only in x-direction, but also in y-direction. Therefore, the general expressions of $\hat{\phi}\left(\underline{\mathbf{x}},\omega\right)$ and $\hat{\underline{\boldsymbol{\psi}}}\left(\underline{\mathbf{x}},\omega\right)$ are:

$$\hat{\phi}\left(\underline{\mathbf{x}},\omega\right) = Ae^{-\mathrm{i}k_x x}e^{-\mathrm{i}k_y y}e^{-\mathrm{i}k_{\mathrm{P}z} z} \tag{15}$$

$$\hat{\underline{\boldsymbol{\psi}}}\left(\underline{\mathbf{x}},\omega\right) = \begin{bmatrix} B & C & D \end{bmatrix}^T e^{-\mathrm{i}k_x x}e^{-\mathrm{i}k_y y}e^{-\mathrm{i}k_{\mathrm{S}z} z} \tag{16}$$

where A, B, C, D are unknown coefficients to be determined by the boundary conditions, k_x is the wavenumber in the x-direction, k_y is the wavenumber in the y-direction, and $k_{\mathrm{P}z}$ and $k_{\mathrm{S}z}$ are respectively the wavenumbers in the z-direction for the P-wave and S-wave. Note that the signs of $k_{\mathrm{P}z}$ and $k_{\mathrm{S}z}$ should be chosen carefully to ensure that the waves propagate and/or attenuate in the positive z-direction. After substituting equations (15) and (16) into equations (13) and (14), the expressions for $k_{\mathrm{P}z}$ and $k_{\mathrm{S}z}$ can be obtained:

$$k_{\mathrm{P}z}^2 = \frac{\left(\omega + ck_x\right)^2}{c_{\mathrm{P}}^2} - k_x^2 - k_y^2 \tag{17}$$

$$k_{\mathrm{S}z}^2 = \frac{\left(\omega + ck_x\right)^2}{c_{\mathrm{S}}^2} - k_x^2 - k_y^2 \tag{18}$$

By substituting equation (12) into the expressions of the constitutive equations in frequency domain, the following relationships between the stresses and the potentials in frequency domain are obtained:

$$\hat{\sigma}_{xx}\left(\underline{\mathbf{x}},\omega\right) = \lambda\left(\frac{\partial^2}{\partial x^2}+\frac{\partial^2}{\partial y^2}+\frac{\partial^2}{\partial z^2}\right)\hat{\phi} + 2\mu\left(\frac{\partial^2\hat{\phi}}{\partial x^2}+\frac{\partial^2\hat{\psi}_z}{\partial x\partial y}-\frac{\partial^2\hat{\psi}_y}{\partial z\partial x}\right) \tag{19}$$

$$\hat{\sigma}_{yy}\left(\underline{\mathbf{x}},\omega\right) = \lambda\left(\frac{\partial^2}{\partial x^2}+\frac{\partial^2}{\partial y^2}+\frac{\partial^2}{\partial z^2}\right)\hat{\phi} + 2\mu\left(\frac{\partial^2\hat{\phi}}{\partial y^2}+\frac{\partial^2\hat{\psi}_x}{\partial y\partial z}-\frac{\partial^2\hat{\psi}_z}{\partial x\partial y}\right) \tag{20}$$

$$\hat{\sigma}_{zz}\left(\underline{\mathbf{x}},\omega\right) = \lambda\left(\frac{\partial^2}{\partial x^2}+\frac{\partial^2}{\partial y^2}+\frac{\partial^2}{\partial z^2}\right)\hat{\phi} + 2\mu\left(\frac{\partial^2\hat{\phi}}{\partial z^2}+\frac{\partial^2\hat{\psi}_y}{\partial z\partial x}-\frac{\partial^2\hat{\psi}_x}{\partial y\partial z}\right) \tag{21}$$

$$\hat{\sigma}_{xy}\left(\underline{\mathbf{x}},\omega\right) = \mu\left[2\frac{\partial^2\hat{\phi}}{\partial x\partial y}+\frac{\partial^2\hat{\psi}_x}{\partial z\partial x}-\frac{\partial^2\hat{\psi}_y}{\partial y\partial z}-\left(\frac{\partial^2}{\partial x^2}-\frac{\partial^2}{\partial y^2}\right)\hat{\psi}_z\right] \tag{22}$$

$$\hat{\sigma}_{yz}\left(\underline{\mathbf{x}},\omega\right)=\mu\left[2\frac{\partial^2\hat{\phi}}{\partial y\partial z}+\frac{\partial^2\hat{\psi}_y}{\partial x\partial y}-\frac{\partial^2\hat{\psi}_z}{\partial z\partial x}-\left(\frac{\partial^2}{\partial y^2}-\frac{\partial^2}{\partial z^2}\right)\hat{\psi}_x\right] \tag{23}$$

$$\hat{\sigma}_{zx}\left(\underline{\mathbf{x}},\omega\right)=\mu\left[2\frac{\partial^2\hat{\phi}}{\partial z\partial x}+\frac{\partial^2\hat{\psi}_z}{\partial y\partial z}-\frac{\partial^2\hat{\psi}_x}{\partial x\partial y}-\left(\frac{\partial^2}{\partial z^2}-\frac{\partial^2}{\partial x^2}\right)\hat{\psi}_y\right] \tag{24}$$

in which $\hat{\psi}_x$, $\hat{\psi}_y$, and $\hat{\psi}_z$ are three components of $\hat{\underline{\boldsymbol{\psi}}}\left(\underline{\mathbf{x}},\omega\right)$.

In addition, by combining the expressions of c_{P} and c_{S} with equations (17) and (18), the relationship between Lamé constants can be obtained:

$$\lambda=-\frac{k_x^2+k_y^2+2k_{\mathrm{Pz}}^2-k_{\mathrm{Sz}}^2}{k_x^2+k_y^2+k_{\mathrm{Pz}}^2}\mu \tag{25}$$

2.3. Spectral element formulation

In the SEM, the response of an element is determined by its total wave field, which is the superposition of wave fields originating from different boundaries (Al-Khoury et al., 2001). In this method, the number of elements needed for a simulation is the same as the number of layers because one element is sufficient to simulate a whole layer, which makes it efficient for dynamic analysis of layered systems. In this section, a layer spectral element and a semi-infinite spectral element are formulated to simulate a layer and a half-space, respectively. The combinations of these two spectral elements are capable of modelling different layered systems.

2.3.1. Layer spectral element

As shown in Figure 3(a), the layer spectral element consists of two parallel horizontal rectangular surfaces, which constrain the waves to propagate within the element. The element vertically covers the whole simulated layer, and it horizontally extends to a certain distance after which the response caused by waves is negligible. In addition, the spectral element of a layer with thickness *h* is physically defined by two nodes located at (0, 0, 0) and (0, 0, *h*), each of which has three degrees of freedom. In the layer spectral element, the total potentials can be expressed as follows (Al-Khoury et al., 2001; van Dalen et al., 2015):

$$\hat{\phi}\left(\underline{\mathbf{x}},\omega\right)=e^{-\mathrm{i}k_x x}e^{-\mathrm{i}k_y y}\left[A_1e^{-\mathrm{i}k_{\mathrm{Pz}}z}+A_2e^{\mathrm{i}k_{\mathrm{Pz}}(z-h)}\right] \tag{26}$$

$$\hat{\underline{\boldsymbol{\psi}}}\left(\underline{\mathbf{x}},\omega\right)=e^{-\mathrm{i}k_x x}e^{-\mathrm{i}k_y y}\begin{bmatrix}B_1e^{-\mathrm{i}k_{\mathrm{S}z}z}+B_2e^{\mathrm{i}k_{\mathrm{S}z}(z-h)}\\C_1e^{-\mathrm{i}k_{\mathrm{S}z}z}+C_2e^{\mathrm{i}k_{\mathrm{S}z}(z-h)}\\D_1e^{-\mathrm{i}k_{\mathrm{S}z}z}+D_2e^{\mathrm{i}k_{\mathrm{S}z}(z-h)}\end{bmatrix} \tag{27}$$

where A_1, A_2, B_1, B_2, C_1, C_2, D_1, and D_2 are the unknown coefficients to be determined by boundary conditions. The first terms are the potentials of the wave fields originated from the top surface, while the second terms are the potentials of the wave fields reflected from the bottom surface.

The Fourier transform is applied to the Gauge condition in the moving coordinate system to obtain its spectral form, which is expressed as follows:

$$\nabla\cdot\hat{\underline{\boldsymbol{\psi}}}\left(\underline{\mathbf{x}},\omega\right)=0 \tag{28}$$

After substituting equation (27) into equation (28), the following relationships are obtained:

$$D_1=-\frac{k_xB_1+k_yC_1}{k_{\mathrm{S}z}} \tag{29}$$

$$D_2=\frac{k_xB_2+k_yC_2}{k_{\mathrm{S}z}} \tag{30}$$

Equations (29) and (30) are substituted into equation (27) first to decrease the number of unknown coefficients. Then equations (26) and (27) are substituted into equation (12) to obtain the expressions for the displacements in frequency domain, which have the following forms:

$$\hat{u}_x\left(\underline{\mathbf{x}},\omega\right)=-\mathrm{i}e^{-\mathrm{i}k_x x}e^{-\mathrm{i}k_y y}\begin{bmatrix}k_x\left(A_1e^{-\mathrm{i}k_{\mathrm{P}z}z}+A_2e^{\mathrm{i}k_{\mathrm{P}z}(z-h)}\right)-\dfrac{k_xk_y}{k_{\mathrm{S}z}}\left(B_1e^{-\mathrm{i}k_{\mathrm{S}z}z}-B_2e^{\mathrm{i}k_{\mathrm{S}z}(z-h)}\right)\\-\dfrac{k_y^2+k_{\mathrm{S}z}^2}{k_{\mathrm{S}z}}\left(C_1e^{-\mathrm{i}k_{\mathrm{S}z}z}-C_2e^{\mathrm{i}k_{\mathrm{S}z}(z-h)}\right)\end{bmatrix} \tag{31}$$

$$\hat{u}_y\left(\underline{\mathbf{x}},\omega\right)=-\mathrm{i}e^{-\mathrm{i}k_x x}e^{-\mathrm{i}k_y y}\begin{bmatrix}k_y\left(A_1e^{-\mathrm{i}k_{\mathrm{P}z}z}+A_2e^{\mathrm{i}k_{\mathrm{P}z}(z-h)}\right)+\dfrac{k_x^2+k_{\mathrm{S}z}^2}{k_{\mathrm{S}z}}\left(B_1e^{-\mathrm{i}k_{\mathrm{S}z}z}-B_2e^{\mathrm{i}k_{\mathrm{S}z}(z-h)}\right)\\+\dfrac{k_xk_y}{k_{\mathrm{S}z}}\left(C_1e^{-\mathrm{i}k_{\mathrm{S}z}z}-C_2e^{\mathrm{i}k_{\mathrm{S}z}(z-h)}\right)\end{bmatrix} \tag{32}$$

$$\hat{u}_z\left(\underline{\mathbf{x}},\omega\right)=-\mathrm{i}e^{-\mathrm{i}k_x x}e^{-\mathrm{i}k_y y}\begin{bmatrix}k_{\mathrm{Pz}}\left(A_1e^{-\mathrm{i}k_{\mathrm{Pz}}z}-A_2e^{\mathrm{i}k_{\mathrm{Pz}}(z-h)}\right)-k_y\left(B_1e^{-\mathrm{i}k_{\mathrm{Sz}}z}+B_2e^{\mathrm{i}k_{\mathrm{Sz}}(z-h)}\right)\\+k_x\left(C_1e^{-\mathrm{i}k_{\mathrm{Sz}}z}+C_2e^{\mathrm{i}k_{\mathrm{Sz}}(z-h)}\right)\end{bmatrix} \quad (33)$$

The displacements of the top node are notated as $\hat{u}_x^1$, $\hat{u}_y^1$, and $\hat{u}_z^1$, and the displacements of the bottom node are notated as $\hat{u}_x^2$, $\hat{u}_y^2$, and $\hat{u}_z^2$. Then, the coordinates of the nodes are substituted into equations (31) to (33) to obtain the nodal displacements, which can be expressed as follows:

$$\underline{\hat{\mathbf{u}}}_0^{\mathrm{e}}=\underline{\underline{\hat{\mathbf{L}}}}^{\mathrm{e}}\cdot\underline{\hat{\mathbf{a}}} \quad (34)$$

in which the superscript "e" means the corresponding quantities are expressed for an element, $\underline{\hat{\mathbf{u}}}_0^{\mathrm{e}}=\begin{bmatrix}\hat{u}_x^1 & \hat{u}_y^1 & \hat{u}_z^1 & \hat{u}_x^2 & \hat{u}_y^2 & \hat{u}_z^2\end{bmatrix}^{\mathrm{T}}$ is the nodal displacement vector of the element, $\underline{\hat{\mathbf{a}}}=\begin{bmatrix}A_1 & A_2 & B_1 & B_2 & C_1 & C_2\end{bmatrix}^{\mathrm{T}}$ is the unknown coefficient vector, and $\underline{\underline{\hat{\mathbf{L}}}}^{\mathrm{e}}$ is a frequency and wavenumber dependent matrix which has the following expression:

$$\underline{\underline{\hat{\mathbf{L}}}}^{\mathrm{e}}=\mathrm{i}\begin{bmatrix}
-k_x & -k_xe^{-\mathrm{i}k_{\mathrm{Pz}}h} & \frac{k_xk_y}{k_{\mathrm{Sz}}} & -\frac{k_xk_y}{k_{\mathrm{Sz}}}e^{-\mathrm{i}k_{\mathrm{Sz}}h} & \frac{k_y^2+k_{\mathrm{Sz}}^2}{k_{\mathrm{Sz}}} & -\frac{k_y^2+k_{\mathrm{Sz}}^2}{k_{\mathrm{Sz}}}e^{-\mathrm{i}k_{\mathrm{Sz}}h}\\
-k_y & -k_ye^{-\mathrm{i}k_{\mathrm{Pz}}h} & -\frac{k_x^2+k_{\mathrm{Sz}}^2}{k_{\mathrm{Sz}}} & \frac{k_x^2+k_{\mathrm{Sz}}^2}{k_{\mathrm{Sz}}}e^{-\mathrm{i}k_{\mathrm{Sz}}h} & -\frac{k_xk_y}{k_{\mathrm{Sz}}} & \frac{k_xk_y}{k_{\mathrm{Sz}}}e^{-\mathrm{i}k_{\mathrm{Sz}}h}\\
-k_{\mathrm{Pz}} & k_{\mathrm{Pz}}e^{-\mathrm{i}k_{\mathrm{Pz}}h} & k_y & k_ye^{-\mathrm{i}k_{\mathrm{Sz}}h} & -k_x & -k_xe^{-\mathrm{i}k_{\mathrm{Sz}}h}\\
-k_xe^{-\mathrm{i}k_{\mathrm{Pz}}h} & -k_x & \frac{k_xk_y}{k_{\mathrm{Sz}}}e^{-\mathrm{i}k_{\mathrm{Sz}}h} & -\frac{k_xk_y}{k_{\mathrm{Sz}}} & \frac{k_y^2+k_{\mathrm{Sz}}^2}{k_{\mathrm{Sz}}}e^{-\mathrm{i}k_{\mathrm{Sz}}h} & -\frac{k_y^2+k_{\mathrm{Sz}}^2}{k_{\mathrm{Sz}}}\\
-k_ye^{-\mathrm{i}k_{\mathrm{Pz}}h} & -k_y & -\frac{k_x^2+k_{\mathrm{Sz}}^2}{k_{\mathrm{Sz}}}e^{-\mathrm{i}k_{\mathrm{Sz}}h} & \frac{k_x^2+k_{\mathrm{Sz}}^2}{k_{\mathrm{Sz}}} & -\frac{k_xk_y}{k_{\mathrm{Sz}}}e^{-\mathrm{i}k_{\mathrm{Sz}}h} & \frac{k_xk_y}{k_{\mathrm{Sz}}}\\
-k_{\mathrm{Pz}}e^{-\mathrm{i}k_{\mathrm{Pz}}h} & k_{\mathrm{Pz}} & k_ye^{-\mathrm{i}k_{\mathrm{Sz}}h} & k_y & -k_xe^{-\mathrm{i}k_{\mathrm{Sz}}h} & -k_x
\end{bmatrix}$$

By substituting equations (26) and (27) into equations (19) to (24) and considering equation (25), the transformed expressions of the stresses can be obtained:

$$\hat{\sigma}_{xx}\left(\underline{\mathbf{x}},\omega\right)=-\mu e^{-\mathrm{i}k_x x}e^{-\mathrm{i}k_y y}\begin{bmatrix}\left(k_x^2-k_y^2-2k_{\mathrm{Pz}}^2+k_{\mathrm{Sz}}^2\right)\left(A_1e^{-\mathrm{i}k_{\mathrm{Pz}}z}+A_2e^{\mathrm{i}k_{\mathrm{Pz}}(z-h)}\right)\\-\frac{2k_x^2k_y}{k_{\mathrm{Sz}}}\left(B_1e^{-\mathrm{i}k_{\mathrm{Sz}}z}-B_2e^{\mathrm{i}k_{\mathrm{Sz}}(z-h)}\right)-\frac{2k_x\left(k_y^2+k_{\mathrm{Sz}}^2\right)}{k_{\mathrm{Sz}}}\left(C_1e^{-\mathrm{i}k_{\mathrm{Sz}}z}-C_2e^{\mathrm{i}k_{\mathrm{Sz}}(z-h)}\right)\end{bmatrix} \quad (35)$$

$$\hat{\sigma}_{yy}\left(\underline{\mathbf{x}},\omega\right)=\mu e^{-\mathrm{i}k_x x}e^{-\mathrm{i}k_y y}\begin{bmatrix}\left(k_x^2-k_y^2+2k_{\mathrm{Pz}}^2-k_{\mathrm{Sz}}^2\right)\left(A_1e^{-\mathrm{i}k_{\mathrm{Pz}}z}+A_2e^{\mathrm{i}k_{\mathrm{Pz}}(z-h)}\right)\\-\dfrac{2k_y\left(k_x^2+k_{\mathrm{Sz}}^2\right)}{k_{\mathrm{Sz}}}\left(B_1e^{-\mathrm{i}k_{\mathrm{Sz}}z}-B_2e^{\mathrm{i}k_{\mathrm{Sz}}(z-h)}\right)-\dfrac{2k_xk_y^2}{k_{\mathrm{Sz}}}\left(C_1e^{-\mathrm{i}k_{\mathrm{Sz}}z}-C_2e^{\mathrm{i}k_{\mathrm{Sz}}(z-h)}\right)\end{bmatrix} \tag{36}$$

$$\hat{\sigma}_{zz}\left(\underline{\mathbf{x}},\omega\right)=\mu e^{-\mathrm{i}k_x x}e^{-\mathrm{i}k_y y}\begin{bmatrix}\left(k_x^2+k_y^2-k_{\mathrm{Sz}}^2\right)\left(A_1e^{-\mathrm{i}k_{\mathrm{Pz}}z}+A_2e^{\mathrm{i}k_{\mathrm{Pz}}(z-h)}\right)\\+2k_yk_{\mathrm{Sz}}\left(B_1e^{-\mathrm{i}k_{\mathrm{Sz}}z}-B_2e^{\mathrm{i}k_{\mathrm{Sz}}(z-h)}\right)-2k_xk_{\mathrm{Sz}}\left(C_1e^{-\mathrm{i}k_{\mathrm{Sz}}z}-C_2e^{\mathrm{i}k_{\mathrm{Sz}}(z-h)}\right)\end{bmatrix} \tag{37}$$

$$\hat{\sigma}_{xy}\left(\underline{\mathbf{x}},\omega\right)=-\mu e^{-\mathrm{i}k_x x}e^{-\mathrm{i}k_y y}\begin{bmatrix}2k_xk_y\left(A_1e^{-\mathrm{i}k_{\mathrm{Pz}}z}+A_2e^{\mathrm{i}k_{\mathrm{Pz}}(z-h)}\right)+\dfrac{k_x\left(k_x^2-k_y^2+k_{\mathrm{Sz}}^2\right)}{k_{\mathrm{Sz}}}\left(B_1e^{-\mathrm{i}k_{\mathrm{Sz}}z}-B_2e^{\mathrm{i}k_{\mathrm{Sz}}(z-h)}\right)\\+\dfrac{k_y\left(k_x^2-k_y^2-k_{\mathrm{Sz}}^2\right)}{k_{\mathrm{Sz}}}\left(C_1e^{-\mathrm{i}k_{\mathrm{Sz}}z}-C_2e^{\mathrm{i}k_{\mathrm{Sz}}(z-h)}\right)\end{bmatrix} \tag{38}$$

$$\hat{\sigma}_{yz}\left(\underline{\mathbf{x}},\omega\right)=-\mu e^{-\mathrm{i}k_x x}e^{-\mathrm{i}k_y y}\begin{bmatrix}2k_yk_{\mathrm{Pz}}\left(A_1e^{-\mathrm{i}k_{\mathrm{Pz}}z}-A_2e^{\mathrm{i}k_{\mathrm{Pz}}(z-h)}\right)+\left(k_x^2-k_y^2+k_{\mathrm{Sz}}^2\right)\left(B_1e^{-\mathrm{i}k_{\mathrm{Sz}}z}+B_2e^{\mathrm{i}k_{\mathrm{Sz}}(z-h)}\right)\\+2k_xk_y\left(C_1e^{-\mathrm{i}k_{\mathrm{Sz}}z}+C_2e^{\mathrm{i}k_{\mathrm{Sz}}(z-h)}\right)\end{bmatrix} \tag{39}$$

$$\hat{\sigma}_{zx}\left(\underline{\mathbf{x}},\omega\right)=-\mu e^{-\mathrm{i}k_x x}e^{-\mathrm{i}k_y y}\begin{bmatrix}2k_xk_{\mathrm{Pz}}\left(A_1e^{-\mathrm{i}k_{\mathrm{Pz}}z}-A_2e^{\mathrm{i}k_{\mathrm{Pz}}(z-h)}\right)-2k_xk_y\left(B_1e^{-\mathrm{i}k_{\mathrm{Sz}}z}+B_2e^{\mathrm{i}k_{\mathrm{Sz}}(z-h)}\right)\\+\left(k_x^2-k_y^2-k_{\mathrm{Sz}}^2\right)\left(C_1e^{-\mathrm{i}k_{\mathrm{Sz}}z}+C_2e^{\mathrm{i}k_{\mathrm{Sz}}(z-h)}\right)\end{bmatrix} \tag{40}$$

Based on the Cauchy stress principle, for a certain surface, the relationship between the surface traction vector $\underline{\mathbf{t}}$ and the Cauchy stress matrix $\underline{\underline{\boldsymbol{\sigma}}}$ can be expressed as follows:

$$\underline{\mathbf{t}}=\underline{\underline{\boldsymbol{\sigma}}}\cdot\underline{\mathbf{n}} \tag{41}$$

where $\underline{\mathbf{n}}$ is the unit outward normal vector of the surface. The tractions of the top node are denoted as $\hat{t}_x^1$, $\hat{t}_y^1$, and $\hat{t}_z^1$, and the tractions of the bottom node are denoted as $\hat{t}_x^2$, $\hat{t}_y^2$, and $\hat{t}_z^2$. On the basis of equation (41), the nodal tractions have the following relationships with the nodal Cauchy stresses:

$$\hat{t}_x^1=-\hat{\sigma}_{zx}^1,\quad \hat{t}_y^1=-\hat{\sigma}_{zy}^1,\quad \hat{t}_z^1=-\hat{\sigma}_{zz}^1 \tag{42}$$

$$\hat{t}_x^2=\hat{\sigma}_{zx}^2,\quad \hat{t}_y^2=\hat{\sigma}_{zy}^2,\quad \hat{t}_z^2=\hat{\sigma}_{zz}^2 \tag{43}$$

in which $\hat{\sigma}_{zx}^1$, $\hat{\sigma}_{zy}^1$, and $\hat{\sigma}_{zz}^1$ are the Cauchy stresses of the top node, and $\hat{\sigma}_{zx}^2$, $\hat{\sigma}_{zy}^2$, and $\hat{\sigma}_{zz}^2$ are the Cauchy stresses of the bottom node.

The nodal coordinates are substituted into equations (35) to (40) to derive the nodal stresses, which are then incorporated into equations (42) and (43) to obtain the

expressions of nodal tractions, which are expressed as:

$$\underline{\hat{\mathbf{t}}}_0^{\mathrm{e}} = \hat{\underline{\underline{\mathbf{H}}}}^{\mathrm{e}} \cdot \underline{\hat{\mathbf{a}}} \tag{44}$$

where $\underline{\hat{\mathbf{t}}}_0^{\mathrm{e}} = \begin{bmatrix} \hat{t}_x^1 & \hat{t}_y^1 & \hat{t}_z^1 & \hat{t}_x^2 & \hat{t}_y^2 & \hat{t}_z^2 \end{bmatrix}^{\mathrm{T}}$ is the nodal traction vector of the element, $\hat{\underline{\underline{\mathbf{H}}}}^{\mathrm{e}}$ is a frequency and wavenumber dependent matrix which has the following form:

$$\hat{\underline{\underline{\mathbf{H}}}}^{\mathrm{e}} = \mu \begin{bmatrix} 2k_x k_{\mathrm{Pz}} & -2k_x k_{\mathrm{Pz}} e^{-\mathrm{i}k_{\mathrm{Pz}}h} & -2k_x k_y & -2k_x k_y e^{-\mathrm{i}k_{\mathrm{Sz}}h} & k_3^2 & k_3^2 e^{-\mathrm{i}k_{\mathrm{Sz}}h} \\ 2k_y k_{\mathrm{Pz}} & -2k_y k_{\mathrm{Pz}} e^{-\mathrm{i}k_{\mathrm{Pz}}h} & k_2^2 & k_2^2 e^{-\mathrm{i}k_{\mathrm{Sz}}h} & 2k_x k_y & 2k_x k_y e^{-\mathrm{i}k_{\mathrm{Sz}}h} \\ -k_1^2 & -k_1^2 e^{-\mathrm{i}k_{\mathrm{Pz}}h} & -2k_y k_{\mathrm{Sz}} & 2k_y k_{\mathrm{Sz}} e^{-\mathrm{i}k_{\mathrm{Sz}}h} & 2k_x k_{\mathrm{Sz}} & -2k_x k_{\mathrm{Sz}} e^{-\mathrm{i}k_{\mathrm{Sz}}h} \\ -2k_x k_{\mathrm{Pz}} e^{-\mathrm{i}k_{\mathrm{Pz}}h} & 2k_x k_{\mathrm{Pz}} & 2k_x k_y e^{-\mathrm{i}k_{\mathrm{Sz}}h} & 2k_x k_y & -k_3^2 e^{-\mathrm{i}k_{\mathrm{Sz}}h} & -k_3^2 \\ -2k_y k_{\mathrm{Pz}} e^{-\mathrm{i}k_{\mathrm{Pz}}h} & 2k_y k_{\mathrm{Pz}} & -k_2^2 e^{-\mathrm{i}k_{\mathrm{Sz}}h} & -k_2^2 & -2k_x k_y e^{-\mathrm{i}k_{\mathrm{Sz}}h} & -2k_x k_y \\ k_1^2 e^{-\mathrm{i}k_{\mathrm{Pz}}h} & k_1^2 & 2k_y k_{\mathrm{Sz}} e^{-\mathrm{i}k_{\mathrm{Sz}}h} & -2k_y k_{\mathrm{Sz}} & -2k_x k_{\mathrm{Sz}} e^{-\mathrm{i}k_{\mathrm{Sz}}h} & 2k_x k_{\mathrm{Sz}} \end{bmatrix}$$

with $k_1^2 = k_x^2 + k_y^2 - k_{\mathrm{Sz}}^2$, $k_2^2 = k_x^2 - k_y^2 + k_{\mathrm{Sz}}^2$, and $k_3^2 = k_x^2 - k_y^2 - k_{\mathrm{Sz}}^2$.

By combining equations (34) and (44), the relationship between the nodal traction vector and the nodal displacement vector is obtained, which can be expressed as:

$$\underline{\hat{\mathbf{t}}}_0^{\mathrm{e}} = \hat{\underline{\underline{\mathbf{k}}}}^{\mathrm{e}} \cdot \underline{\hat{\mathbf{u}}}_0^{\mathrm{e}} \tag{45}$$

in which $\hat{\underline{\underline{\mathbf{k}}}}^{\mathrm{e}} = \hat{\underline{\underline{\mathbf{H}}}}^{\mathrm{e}} \cdot \left(\hat{\underline{\underline{\mathbf{L}}}}^{\mathrm{e}} \right)^{-1}$ can be regarded as the element stiffness matrix, and the detailed expressions of its components are shown in Appendix B.

2.3.2. Semi-infinite spectral element

As shown in Figure 3(b), the semi-infinite spectral element is composed of a horizontal rectangular surface, and physically defined by a node located at (0, 0, 0) with three degrees of freedom. In the semi-infinite spectral element, the waves originated from the surface travel in the positive *z*-direction and no reflection occurs, which physically means that the energy is radiated away. Actually, the semi-infinite spectral element can be regarded as a special case of the layer spectral element that only contains the top surface, which requires the coefficients of A_2, B_2, C_2, and D_2 in equations (26) and (27) to be zero. Accordingly, the transformed displacements for the semi-infinite spectral element can be expressed as follows:

$$\hat{u}_x\left(\underline{\mathbf{x}},\omega\right)=-\mathrm{i}e^{-\mathrm{i}k_x x}e^{-\mathrm{i}k_y y}\left(k_x A_1 e^{-\mathrm{i}k_{\mathrm{P}z} z}-\frac{k_x k_y}{k_{\mathrm{S}z}}B_1 e^{-\mathrm{i}k_{\mathrm{S}z} z}-\frac{k_y^2+k_{\mathrm{S}z}^2}{k_{\mathrm{S}z}}C_1 e^{-\mathrm{i}k_{\mathrm{S}z} z}\right) \tag{46}$$

$$\hat{u}_y\left(\underline{\mathbf{x}},\omega\right)=-\mathrm{i}e^{-\mathrm{i}k_x x}e^{-\mathrm{i}k_y y}\left(k_y A_1 e^{-\mathrm{i}k_{\mathrm{P}z} z}+\frac{k_x^2+k_{\mathrm{S}z}^2}{k_{\mathrm{S}z}}B_1 e^{-\mathrm{i}k_{\mathrm{S}z} z}+\frac{k_x k_y}{k_{\mathrm{S}z}}C_1 e^{-\mathrm{i}k_{\mathrm{S}z} z}\right) \tag{47}$$

$$\hat{u}_z\left(\underline{\mathbf{x}},\omega\right)=-\mathrm{i}e^{-\mathrm{i}k_x x}e^{-\mathrm{i}k_y y}\left(k_{\mathrm{P}z} A_1 e^{-\mathrm{i}k_{\mathrm{P}z} z}-k_y B_1 e^{-\mathrm{i}k_{\mathrm{S}z} z}+k_x C_1 e^{-\mathrm{i}k_{\mathrm{S}z} z}\right) \tag{48}$$

After substituting the coordinates of the node, the nodal displacements can be expressed as:

$$\begin{bmatrix}\hat{u}_x^1\\ \hat{u}_y^1\\ \hat{u}_z^1\end{bmatrix}=\mathrm{i}\begin{bmatrix}-k_x & \frac{k_x k_y}{k_{\mathrm{S}z}} & \frac{k_y^2+k_{\mathrm{S}z}^2}{k_{\mathrm{S}z}}\\ -k_y & -\frac{k_x^2+k_{\mathrm{S}z}^2}{k_{\mathrm{S}z}} & -\frac{k_x k_y}{k_{\mathrm{S}z}}\\ -k_{\mathrm{P}z} & k_y & -k_x\end{bmatrix}\begin{bmatrix}A_1\\ B_1\\ C_1\end{bmatrix} \tag{49}$$

The stresses in frequency domain become:

$$\hat{\sigma}_{xx}\left(\underline{\mathbf{x}},\omega\right)=-\mu e^{-\mathrm{i}k_x x}e^{-\mathrm{i}k_y y}\begin{bmatrix}\left(k_x^2-k_y^2-2k_{\mathrm{P}z}^2+k_{\mathrm{S}z}^2\right)A_1 e^{-\mathrm{i}k_{\mathrm{P}z} z}\\ -\frac{2k_x^2 k_y}{k_{\mathrm{S}z}}B_1 e^{-\mathrm{i}k_{\mathrm{S}z} z}-\frac{2k_x\left(k_y^2+k_{\mathrm{S}z}^2\right)}{k_{\mathrm{S}z}}C_1 e^{-\mathrm{i}k_{\mathrm{S}z} z}\end{bmatrix} \tag{50}$$

$$\hat{\sigma}_{yy}\left(\underline{\mathbf{x}},\omega\right)=\mu e^{-\mathrm{i}k_x x}e^{-\mathrm{i}k_y y}\begin{bmatrix}\left(k_x^2-k_y^2+2k_{\mathrm{P}z}^2-k_{\mathrm{S}z}^2\right)A_1 e^{-\mathrm{i}k_{\mathrm{P}z} z}\\ -\frac{2k_y\left(k_x^2+k_{\mathrm{S}z}^2\right)}{k_{\mathrm{S}z}}B_1 e^{-\mathrm{i}k_{\mathrm{S}z} z}-\frac{2k_x k_y^2}{k_{\mathrm{S}z}}C_1 e^{-\mathrm{i}k_{\mathrm{S}z} z}\end{bmatrix} \tag{51}$$

$$\hat{\sigma}_{zz}\left(\underline{\mathbf{x}},\omega\right)=\mu e^{-\mathrm{i}k_x x}e^{-\mathrm{i}k_y y}\left[\left(k_x^2+k_y^2-k_{\mathrm{S}z}^2\right)A_1 e^{-\mathrm{i}k_{\mathrm{P}z} z}+2k_y k_{\mathrm{S}z}B_1 e^{-\mathrm{i}k_{\mathrm{S}z} z}-2k_x k_{\mathrm{S}z}C_1 e^{-\mathrm{i}k_{\mathrm{S}z} z}\right] \tag{52}$$

$$\hat{\sigma}_{xy}\left(\underline{\mathbf{x}},\omega\right)=-\mu e^{-\mathrm{i}k_x x}e^{-\mathrm{i}k_y y}\begin{bmatrix}2k_x k_y A_1 e^{-\mathrm{i}k_{\mathrm{P}z} z}+\frac{k_x\left(k_x^2-k_y^2+k_{\mathrm{S}z}^2\right)}{k_{\mathrm{S}z}}B_1 e^{-\mathrm{i}k_{\mathrm{S}z} z}\\ +\frac{k_y\left(k_x^2-k_y^2-k_{\mathrm{S}z}^2\right)}{k_{\mathrm{S}z}}C_1 e^{-\mathrm{i}k_{\mathrm{S}z} z}\end{bmatrix} \tag{53}$$

$$\hat{\sigma}_{yz}\left(\underline{\mathbf{x}},\omega\right)=-\mu e^{-\mathrm{i}k_x x}e^{-\mathrm{i}k_y y}\left[2k_y k_{\mathrm{P}z}A_1 e^{-\mathrm{i}k_{\mathrm{P}z} z}+\left(k_x^2-k_y^2+k_{\mathrm{S}z}^2\right)B_1 e^{-\mathrm{i}k_{\mathrm{S}z} z}+2k_x k_y C_1 e^{-\mathrm{i}k_{\mathrm{S}z} z}\right] \tag{54}$$

$$\hat{\sigma}_{zx}\left(\underline{\mathbf{x}},\omega\right)=-\mu e^{-\mathrm{i}k_x x}e^{-\mathrm{i}k_y y}\left[2k_x k_{\mathrm{P}z}A_1 e^{-\mathrm{i}k_{\mathrm{P}z} z}-2k_x k_y B_1 e^{-\mathrm{i}k_{\mathrm{S}z} z}+\left(k_x^2-k_y^2-k_{\mathrm{S}z}^2\right)C_1 e^{-\mathrm{i}k_{\mathrm{S}z} z}\right] \tag{55}$$

After substituting the nodal coordinates and considering equation (42), the nodal

traction vector is expressed as:

$$\begin{bmatrix} \hat{t}_x^1 \\ \hat{t}_y^1 \\ \hat{t}_z^1 \end{bmatrix} = \mu \begin{bmatrix} 2k_x k_{\mathrm{Pz}} & -2k_x k_y & k_x^2 - k_y^2 - k_{\mathrm{Sz}}^2 \\ 2k_y k_{\mathrm{Pz}} & k_x^2 - k_y^2 + k_{\mathrm{Sz}}^2 & 2k_x k_y \\ -k_x^2 - k_y^2 + k_{\mathrm{Sz}}^2 & -2k_y k_{\mathrm{Sz}} & 2k_x k_{\mathrm{Sz}} \end{bmatrix} \begin{bmatrix} A_1 \\ B_1 \\ C_1 \end{bmatrix} \tag{56}$$

By combining equations (49) and (56), the relationship between the nodal traction vector and the nodal displacement vector is obtained:

$$\begin{bmatrix} \hat{t}_x^1 \\ \hat{t}_y^1 \\ \hat{t}_z^1 \end{bmatrix} = \mathrm{i}\mu \begin{bmatrix} \dfrac{\left(k_x^2 + k_{\mathrm{Sz}}^2\right)k_{\mathrm{Pz}} + k_y^2 k_{\mathrm{Sz}}}{k_x^2 + k_y^2 + k_{\mathrm{Pz}} k_{\mathrm{Sz}}} & \dfrac{k_x k_y \left(k_{\mathrm{Pz}} - k_{\mathrm{Sz}}\right)}{k_x^2 + k_y^2 + k_{\mathrm{Pz}} k_{\mathrm{Sz}}} & \dfrac{k_x k_0^2}{k_x^2 + k_y^2 + k_{\mathrm{Pz}} k_{\mathrm{Sz}}} \\ \dfrac{k_x k_y \left(k_{\mathrm{Pz}} - k_{\mathrm{Sz}}\right)}{k_x^2 + k_y^2 + k_{\mathrm{Pz}} k_{\mathrm{Sz}}} & \dfrac{\left(k_y^2 + k_{\mathrm{Sz}}^2\right)k_{\mathrm{Pz}} + k_x^2 k_{\mathrm{Sz}}}{k_x^2 + k_y^2 + k_{\mathrm{Pz}} k_{\mathrm{Sz}}} & \dfrac{k_y k_0^2}{k_x^2 + k_y^2 + k_{\mathrm{Pz}} k_{\mathrm{Sz}}} \\ -\dfrac{k_x k_0^2}{k_x^2 + k_y^2 + k_{\mathrm{Pz}} k_{\mathrm{Sz}}} & -\dfrac{k_y k_0^2}{k_x^2 + k_y^2 + k_{\mathrm{Pz}} k_{\mathrm{Sz}}} & \dfrac{\left(k_x^2 + k_y^2 + k_{\mathrm{Sz}}^2\right)k_{\mathrm{Sz}}}{k_x^2 + k_y^2 + k_{\mathrm{Pz}} k_{\mathrm{Sz}}} \end{bmatrix} \begin{bmatrix} \hat{u}_x^1 \\ \hat{u}_y^1 \\ \hat{u}_z^1 \end{bmatrix} \tag{57}$$

with $k_0^2 = k_x^2 + k_y^2 + 2k_{\mathrm{Pz}} k_{\mathrm{Sz}} - k_{\mathrm{Sz}}^2$.

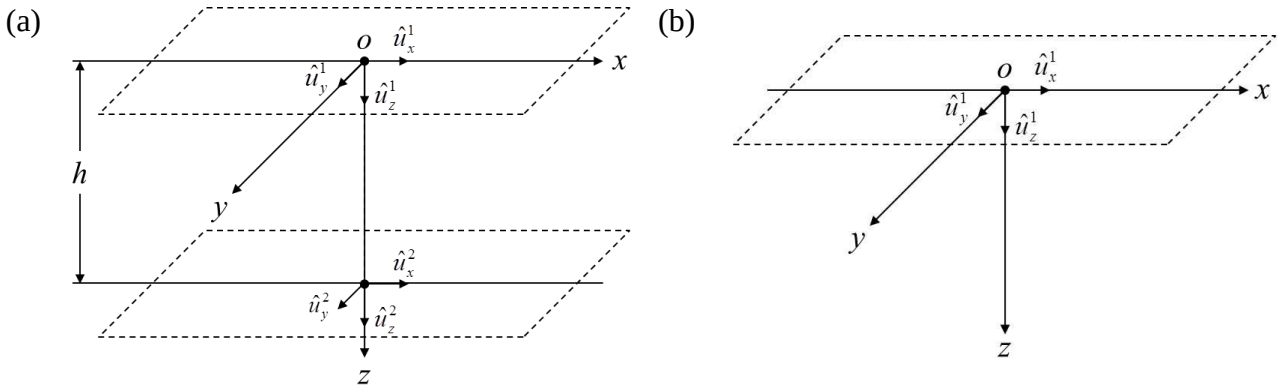

Figure 3. Schematic representation of spectral elements: (a) Layer spectral element and (b) Semi-infinite spectral element.

2.4. Boundary conditions

As shown in Figure 2, the external load is applied on the surface of the layered system in the positive *Z*-direction. The load is assumed to be a uniformly distributed traction over a rectangular area, the amplitude of the load varies with time. In the moving coordinate system, the loading area is fixed and it can be expressed as follows:

$$p_z(x, y, t) = h_0(x, y)\, p(t) \tag{58}$$

where $p_z(x, y, t)$ is the traction applied in the positive *z*-direction, $h_0(x, y)$ is the

spatial distribution function of the traction without dimension, $p(t)$ is the loading history function of the traction with dimension of force/area.

The spatial distribution function $h_0(x,y)$ can be expressed as follows:

$$h_0(x,y) = H(x_0 - |x|)H(y_0 - |y|) \tag{59}$$

in which $H(\cdot)$ is the Heaviside function, $2x_0$ is the length of the loading area in the *x*-direction, and $2y_0$ is the width of the loading area in the *y*-direction.

According to equations (35) to (41), the distribution of tractions on the horizontal surfaces is in the form of $e^{-ik_x x}e^{-ik_y y}$, so $h_0(x,y)$ should be expressed in the same form to match the traction conditions. This can be achieved by using the Fourier series representation:

$$h_0(x,y) = \sum_m \sum_n \tilde{h}_{xm}\tilde{h}_{yn}e^{-ik_{xm}x}e^{-ik_{yn}y} \tag{60}$$

where *m* is an integer that ranges from *–M* to *M* and *n* is an integer that ranges from *–N* to *N*, where *M* and *N* should be large enough to ensure the accuracy of the representation. In addition, $k_{xm} = m\pi/X_0$ and $k_{yn} = n\pi/Y_0$, where $2X_0$ is the length of the space window of interest in the *x*-direction, and $2Y_0$ is the corresponding width in the *y*-direction. The dimensions of the space window should be large enough to cover the influencing area of the applied load. The $\tilde{h}_{xm}$ and $\tilde{h}_{yn}$ are the Fourier coefficients defined as follows:

$$\tilde{h}_{xm} = \frac{1}{2X_0}\int_{-X_0}^{X_0} H(x_0 - |x|)e^{ik_{xm}x}dx \tag{61}$$

$$\tilde{h}_{yn} = \frac{1}{2Y_0}\int_{-Y_0}^{Y_0} H(y_0 - |y|)e^{ik_{yn}y}dy \tag{62}$$

The moving load considered in this paper is harmonically varying, hence the loading history function $p(t)$ can be expressed as follows:

$$p(t) = p_0 e^{i\omega_0 t} \tag{63}$$

in which p_0 is the amplitude of the traction, $\omega_0 = 2\pi f_0$ with ω_0 being the loading angular frequency and f_0 being the loading frequency. By applying the forward Fourier transform based on equation (10), the expression of $p(t)$ in the frequency domain is obtained:

$$\hat{p}(\omega) = p_0 \delta(\omega - \omega_0) \tag{64}$$

where $\delta(\cdot)$ is the Dirac delta function.

Hence, the Fourier transformed expression of the applied surface traction is:

$$\hat{p}_z(x, y, \omega) = \hat{p}(\omega) \sum_m \sum_n \tilde{h}_{xm} \tilde{h}_{yn} e^{-\mathrm{i}k_{xm}x} e^{-\mathrm{i}k_{yn}y} \tag{65}$$

In addition, it can be concluded from equation (65) that the expressions of the potentials should be represented as summations over all k_{xm} and k_{yn} to match the traction conditions.

2.5. Solution scheme

According to the SEM, the combination of several layer spectral elements on top of a semi-infinite spectral element is capable of simulating a layered system. The numbering and assembling of these elements follow the same procedure as in the traditional FEM. However, because of the wavenumber dependence of the element stiffness matrix in the SEM, the whole assembly process is done for each wavenumber combination. The total number of the nodes in the spectral element model of a layered system is notated as *l*, and the global system of equations for a certain wavenumber combination can be expressed as:

$$\hat{\underline{\mathbf{T}}}_0^{mn}(\omega) = \hat{\underline{\underline{\mathbf{K}}}}^{mn}(\omega) \cdot \hat{\underline{\mathbf{U}}}_0^{mn}(\omega) \tag{66}$$

in which the superscript "*mn*" indicates that the quantities correspond to a certain wavenumber combination of k_{xm} and k_{yn}, $\hat{\underline{\mathbf{T}}}_0^{mn}(\omega)$ is the global nodal traction vector with dimensions 3*l* by 1, $\hat{\underline{\underline{\mathbf{K}}}}^{mn}(\omega)$ is the global stiffness matrix with dimensions 3*l* by 3*l*, and $\hat{\underline{\mathbf{U}}}_0^{mn}(\omega)$ is the global nodal displacement vector with dimensions 3*l* by 1.

According to equation (65), the traction of the top node can be expressed as follows:

$$\hat{p}_z\left(0,0,\omega\right)=\hat{p}\left(\omega\right)\sum_m\sum_n\tilde{h}_{xm}\tilde{h}_{yn} \tag{67}$$

Therefore, the global nodal traction vector for a certain wavenumber combination can be expressed as follows:

$$\underline{\hat{\mathbf{T}}}_0^{mn}\left(\omega\right)=\hat{p}\left(\omega\right)\tilde{h}_{xm}\tilde{h}_{yn}\underline{\mathbf{e}}_3 \tag{68}$$

where $\underline{\mathbf{e}}_3$ is a 3l by 1 unit vector with the third component being 1.

According to equation (66), the global nodal displacement vector for a certain wavenumber combination is calculated by:

$$\underline{\hat{\mathbf{U}}}_0^{mn}\left(\omega\right)=\hat{p}\left(\omega\right)\tilde{h}_{xm}\tilde{h}_{yn}\underline{\underline{\hat{\mathbf{G}}}}^{mn}\left(\omega\right)\cdot\underline{\mathbf{e}}_3 \tag{69}$$

in which $\underline{\underline{\hat{\mathbf{G}}}}^{mn}\left(\omega\right)$, the inverse of $\underline{\underline{\hat{\mathbf{K}}}}^{mn}\left(\omega\right)$, can be regarded as the transfer matrix. The nodal displacement vectors for different wavenumber combinations are summed to obtain the total nodal displacement vector caused by the applied load, such that:

$$\underline{\hat{\mathbf{U}}}_0\left(\omega\right)=\hat{p}\left(\omega\right)\sum_m\sum_n\tilde{h}_{xm}\tilde{h}_{yn}\underline{\underline{\hat{\mathbf{G}}}}^{mn}\left(\omega\right)\cdot\underline{\mathbf{e}}_3 \tag{70}$$

where $\underline{\hat{\mathbf{U}}}_0\left(\omega\right)$ is the total nodal displacement vector. Then, the inverse Fourier transform is used to obtain the nodal displacements in time domain, which can be expressed as:

$$\underline{\mathbf{U}}_0\left(t\right)=p_0e^{\mathrm{i}\omega_0t}\sum_m\sum_n\tilde{h}_{xm}\tilde{h}_{yn}\underline{\underline{\hat{\mathbf{G}}}}^{mn}\left(\omega_0\right)\cdot\underline{\mathbf{e}}_3 \tag{71}$$

According to equations (31) to (33), for a certain wavenumber combination, the displacement vector of the horizontal plane where a node is located equals the product of the nodal displacement vector and the term $e^{-\mathrm{i}k_{xm}x}e^{-\mathrm{i}k_{yn}y}$. Therefore, the displacements of points on the nodal horizontal planes can be calculated as:

$$\underline{\mathbf{U}}_0^{\mathrm{plane}}\left(x,y,t\right)=p_0e^{\mathrm{i}\omega_0t}\sum_m\sum_n\tilde{h}_{xm}\tilde{h}_{yn}e^{-\mathrm{i}k_{xm}x}e^{-\mathrm{i}k_{yn}y}\underline{\underline{\hat{\mathbf{G}}}}^{mn}\left(\omega_0\right)\cdot\underline{\mathbf{e}}_3 \tag{72}$$

in which $\underline{\mathbf{U}}_0^{\mathrm{plane}}\left(x,y,t\right)$ is a vector with dimensions 3l by 1, which contains the displacement components of all the horizontal planes where nodes are located.

If the displacement field in a specific layer is desired, the following steps can be

followed. Firstly, one obtains the nodal displacement vector of this layer for a certain wavenumber combination from equation (69). Secondly, one calculates the corresponding coefficient vector via equation (34). Then, one substitutes these coefficients into equations (31) to (33) and sums over all the wavenumber combinations to compute the total displacement field in frequency domain. Finally, one applies the inverse Fourier transform via equation (11) to obtain the total displacement field within this layer in time domain. Corresponding stress and strain fields can also be calculated using the constitutive equations. The procedure to determine the response fields in a half-space is the same as that for a layer. It should be highlighted that all the calculated response fields are steady-state solutions, so they are changing over time with the same frequency as the applied load. For a certain response field (displacement field, stress field, or strain field), it can be expressed as follows:

$$\underline{\mathbf{f}}\left(\underline{\mathbf{x}},t\right)=\underline{\mathbf{F}}\left(\underline{\mathbf{x}},\omega_0\right)e^{\mathrm{i}\omega_0 t} \tag{73}$$

where $\underline{\mathbf{f}}\left(\underline{\mathbf{x}},t\right)$ is a certain response field, $\underline{\mathbf{F}}\left(\underline{\mathbf{x}},\omega_0\right)$ is the corresponding time-independent quantity which is normally complex-valued.

For different loading history functions, a certain component of the response field vector has different forms:

$$f_k\left(\underline{\mathbf{x}},t\right)=\begin{cases}\mathrm{Re}\left[F_k\left(\underline{\mathbf{x}},\omega_0\right)e^{\mathrm{i}\omega_0 t}\right], & p\left(t\right)=p_0\cos\left(\omega_0 t\right)\\ \mathrm{Im}\left[F_k\left(\underline{\mathbf{x}},\omega_0\right)e^{\mathrm{i}\omega_0 t}\right], & p\left(t\right)=p_0\sin\left(\omega_0 t\right)\end{cases} \tag{74}$$

in which the subscript "*k*" represents the considered component of the corresponding vector, $\mathrm{Re}\left(\cdot\right)$ denotes the real part of a complex term, and $\mathrm{Im}\left(\cdot\right)$ denotes the imaginary part of a complex term.

Assuming the loading history is in cosine form, equation (74) can be rewritten as follows accordingly:

$$f_k\left(\underline{\mathbf{x}},t\right)=\mathrm{Re}\left[F_k\left(\underline{\mathbf{x}},\omega_0\right)\right]\cos\left(\omega_0 t\right)-\mathrm{Im}\left[F_k\left(\underline{\mathbf{x}},\omega_0\right)\right]\sin\left(\omega_0 t\right) \tag{75}$$

Equation (75) indicates that a response field component equals to the real part (or imaginary part) of corresponding time-independent quantity at a specific time. In addition, equation (75) can also be written as:

$$f_k\left(\underline{\mathbf{x}},t\right)=\left|F_k\left(\underline{\mathbf{x}},\omega_0\right)\right|\cos\left[\omega_0 t+\theta_k\left(\underline{\mathbf{x}},\omega_0\right)\right] \tag{76}$$

where $\left|F_k\left(\underline{\mathbf{x}},\omega_0\right)\right|$ is the amplitude of vibration, and $\theta_k\left(\underline{\mathbf{x}},\omega_0\right)$ is the corresponding phase angle which satisfies $\tan\left[\theta_k\left(\underline{\mathbf{x}},\omega_0\right)\right]=\dfrac{\mathrm{Im}\left[F_k\left(\underline{\mathbf{x}},\omega_0\right)\right]}{\mathrm{Re}\left[F_k\left(\underline{\mathbf{x}},\omega_0\right)\right]}$.

It can be concluded from equation (76) that, in the moving coordinate system, any response quantity of a point is harmonically varying with the same frequency as the applied load, but different points have different amplitudes and phase angles, which consequently forms a periodically varying profile over time. In this paper, all the results are presented in the moving coordinate system; corresponding results in the stationary coordinate system can be obtained based on the relationship between the coordinates. Working in the moving or stationary coordinate system should give equivalent solutions, because the physical nature of the problem is coordinate system independent (Louhghalam et al., 2013).

Although the presented model is formulated for elastic layered systems, it can be combined with different damping models to simulate layered systems with damping. Note that the damping models should be transformed to the moving coordinate system. Additionally, the presented model can handle different types of surface moving loads by changing the spatial distribution function and the loading history function of the applied load. In this paper, a hysteretic damping model defined in the frequency-wavenumber domain related to the moving coordinate system is used to simulate the damping effect in the system by replacing Young's modulus E with $E[1+\mathrm{i}\eta\mathrm{sgn}(\omega+ck_x)]$, in which η is the loss factor and sgn(·) is the signum function. In addition, in view of the practical speeds of vehicles on roadways, all the considered velocities of the load are taken smaller than the Rayleigh wave speed in layered systems.

3. Model validation

The accuracy of the presented model is validated in this section. At first, this model is implemented in a computer program to compute the response of a layered system by executing the following steps:

(1) For every wavenumber combination, it calculates the element stiffness matrices and assembles them to the global stiffness matrix;

(2) It applies the boundary conditions and computes the global nodal

displacement vector by solving the corresponding global system of equations;

(3) It calculates the response field within a certain layer on the basis of the nodal displacements and obtains the total response field by summing all the contributions at different wavenumbers.

Then, two cases are used to compare the simulated results with corresponding boundary element solutions given by Andersen and Nielsen (2003). These two cases consider the surface deflections of a homogeneous half-space and a layered system caused by a moving harmonic rectangular load. The points along the *x*-axis on the surface are considered in the result comparison, where specifically the corresponding amplitudes and phase angles of displacements in *z*-direction $u_z\left(\underline{\mathbf{x}},t\right)$ are analysed. Note that the loading amplitude used in the current paper is 10^6 times that in the reference literature to make the results comparable with realistic pavement response.

Finally, the proposed model is validated by comparing simulated results with field measurements. A pavement testing facility called LINTRACK (for more details see Appendix C) was used to measure the strains of a pavement structure. The measured maximum longitudinal strains (in moving direction) of the pavement structure are used for comparison with corresponding simulated results.

3.1. Response of a homogeneous half-space under a moving harmonic load

This case considers the dynamic response of a homogeneous half-space caused by a harmonically varying load moving on its surface. The load is uniformly distributed over an area of 3 by 3 m^2, and the amplitude is 1/9 MPa (instead of 1/9 Pa in the literature). The load varies at frequency of 40 Hz and moves in the positive direction of the *x*-axis with velocities of 0, 50, 100 and 150 m/s. The structural parameter values of the half-space are shown in Table 1, these parameter values are corresponding to some unsaturated sandy soil with moderate stiffness. With considering the practical speeds of vehicles on roadways, all the moving velocities of the load considered in this paper are smaller than the Rayleigh wave speed in the layered systems.

Table 1 Structural parameter values of the half-space

Layer	ρ	E	ν	η	h
	kg/m^3	MPa	-	-	m
1	1550	369	0.257	0.1	Infinite

The amplitudes and phase angles of the displacements in *z*-direction $u_z\left(\underline{\mathbf{x}},t\right)$ for points along the *x*-axis on the surface of the half-space are calculated by the presented SEM-based model. In order to obtain converged solutions, 4096×4096 wavenumbers are used, and this holds for all the results shown in this paper. The simulated results are compared with those given in the reference literature (Andersen and Nielsen, 2003) in Figure 4. The comparison shows that the results calculated by these two methods are almost identical for different moving velocities, which proves the accuracy of the proposed semi-infinite spectral element. In addition, some observations can be made:

(1) When the load does not move, the displacement amplitude curve along the *x*-axis is symmetric with respect to $x = 0$ and the displacement amplitude is maximum at $x = 0$.

(2) When the load moves, the displacement amplitude curve along *x*-axis is asymmetric with respect to $x = 0$. The displacement amplitudes at the points in front of the load decrease more rapidly than on the other side, and this trend is more obvious if the moving velocity is higher.

(3) When the moving velocity is increased, the position of the peak of the displacement amplitude curve along the *x*-axis shifts to the left, and the maximum value is slightly higher.

(4) When the moving velocity is zero, the phase angle curve along the *x*-axis is symmetric with respect to $x = 0$. However, with increasing moving velocity, the phase angles of u_z at points in front of the loading area change more rapidly, and consequently the phase angle curve is denser on this side.

(a)

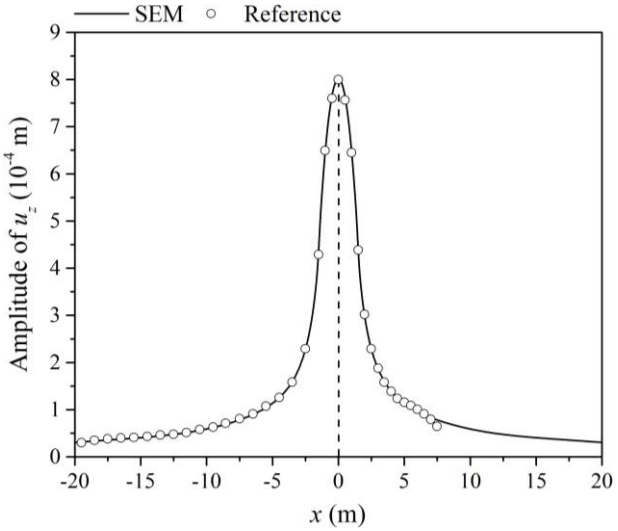
SEM
Reference
Amplitude of u_z (10^{-4} m)
x (m)

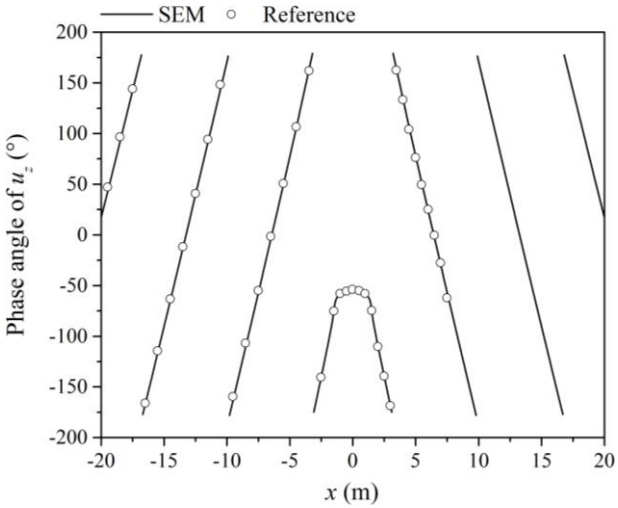
SEM
Reference
Phase angle of u_z (°)
x (m)

(b)

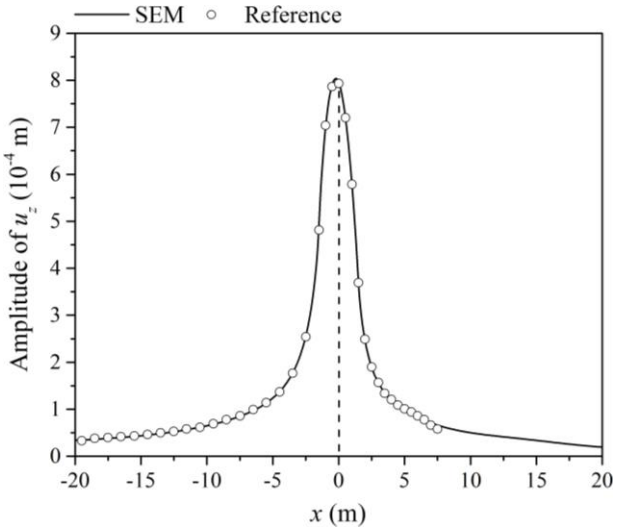
SEM
Reference
Amplitude of u_z (10^{-4} m)
x (m)

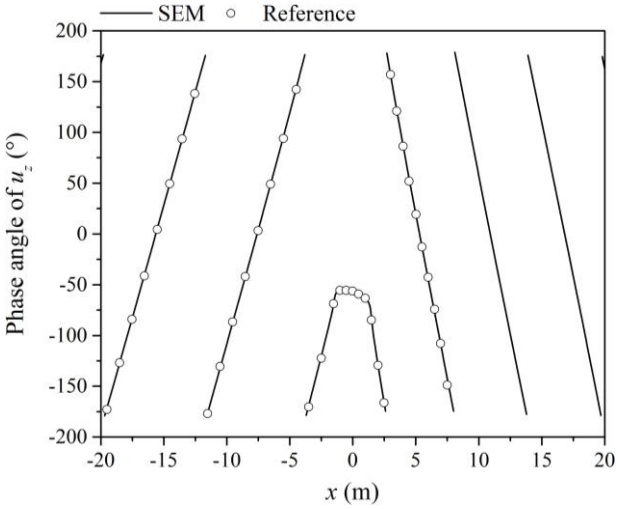
SEM
Reference
Phase angle of u_z (°)
x (m)

(c)

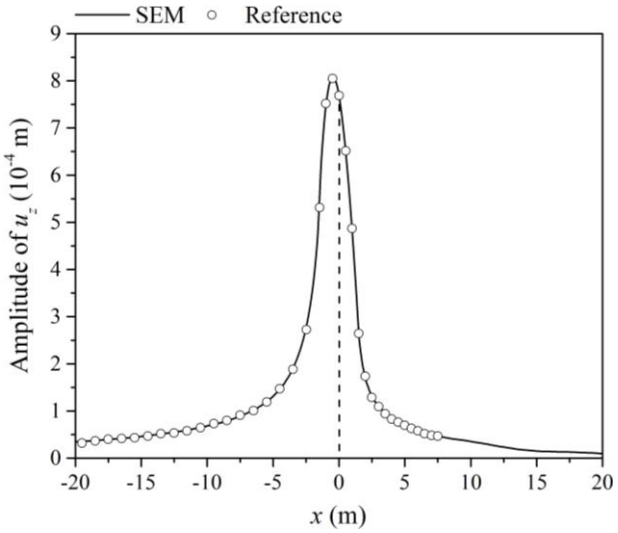
SEM
Reference
Amplitude of u_z (10^{-4} m)
x (m)

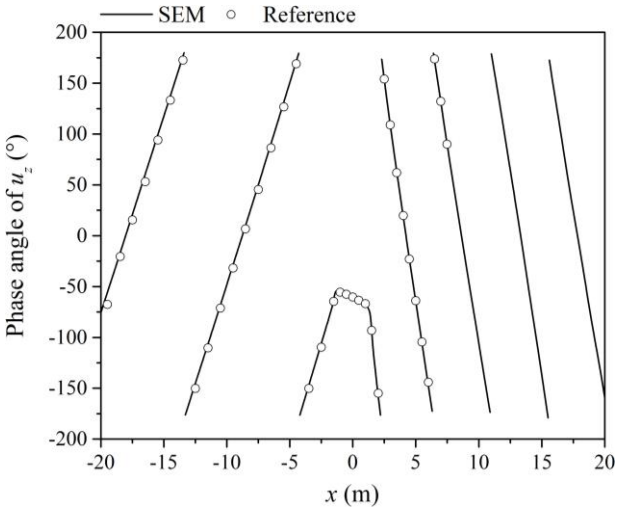
SEM
Reference
Phase angle of u_z (°)
x (m)

(d)

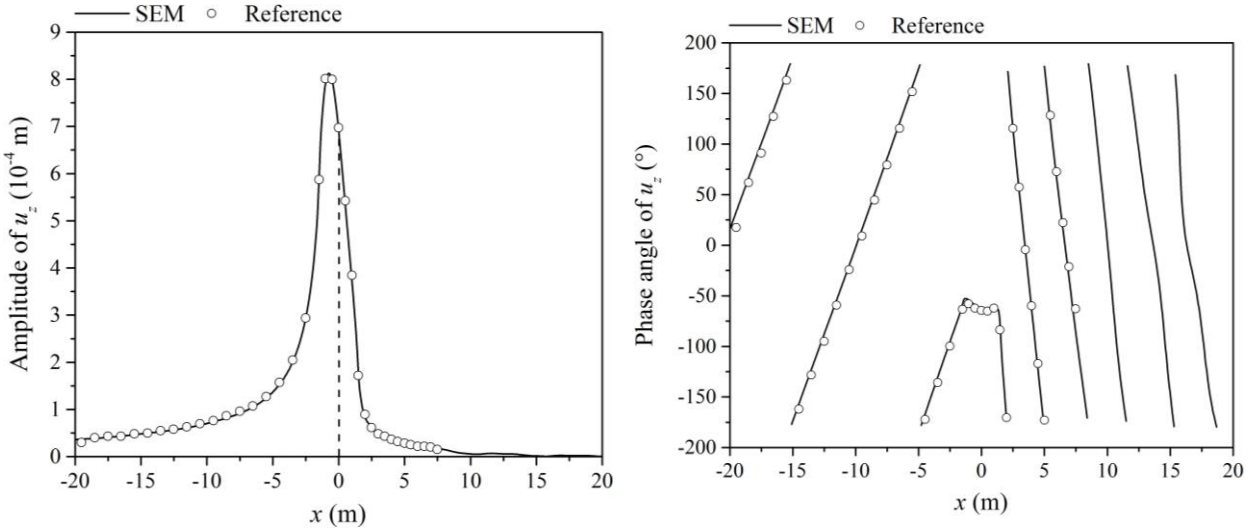

Figure 4. Comparison of u_z for points along the x-axis on the half-space surface calculated by different methods at different moving velocities: (a) c = 0 m/s, (b) c = 50 m/s, (c) c = 100 m/s, and (d) c = 150 m/s.

3.2. Response of a layered system under a moving harmonic load

This case considers the dynamic response of a layered system caused by a uniformly distributed harmonic load moving on its surface. The loading area and amplitude are the same as those in the case of the half-space, while the loading frequency is 20 Hz and the moving velocities are 0, 25, 50, and 75 m/s in the positive direction of the x-axis. The layered system is composed of a horizontal layer with a certain thickness and a homogeneous half-space. The structural parameter values of the layered system are shown in Table 2. The parameter values of this layered system correspond to two kinds of soil, and the soil in the layer is softer than that in the half-space.

Table 2 Structural parameter values of the layered system

Layers	ρ	E	v	η	h
	kg/m^3	MPa	-	-	m
1	1500	100	0.40	0.1	2.0
2	2000	300	0.45	0.1	Infinite

The displacements in the z-direction $u_z\left(\underline{\mathbf{x}},t\right)$ at points along the x-axis on the surface of the layered system are computed by the presented SEM-based model, and the corresponding amplitudes and phase angles are compared with those given in the reference literature (Andersen and Nielsen, 2003) in Figure 5. The comparison indicates that the results calculated by the different methods have good agreement for

different moving velocities, which confirms the accuracy of the proposed layer spectral element and its combination with semi-infinite spectral element. Additionally, some observations can be made:

(1) The displacement amplitude curves along the *x*-axis on the layered system surface have similar changing trends as in the case of homogeneous half-space if the moving velocity is increased. However, the curves have some fluctuations for the layered system, which might be attributed to the complicated wave field in the layer spectral element. The half-space has higher stiffness than the layer above it, so the contribution of the reflected waves is pronounced.

(2) The phase angle curves along the *x*-axis on the layered system surface are more complicated, but the changing trends are similar to the case of homogeneous half-space when the moving velocity is increased.

(a)

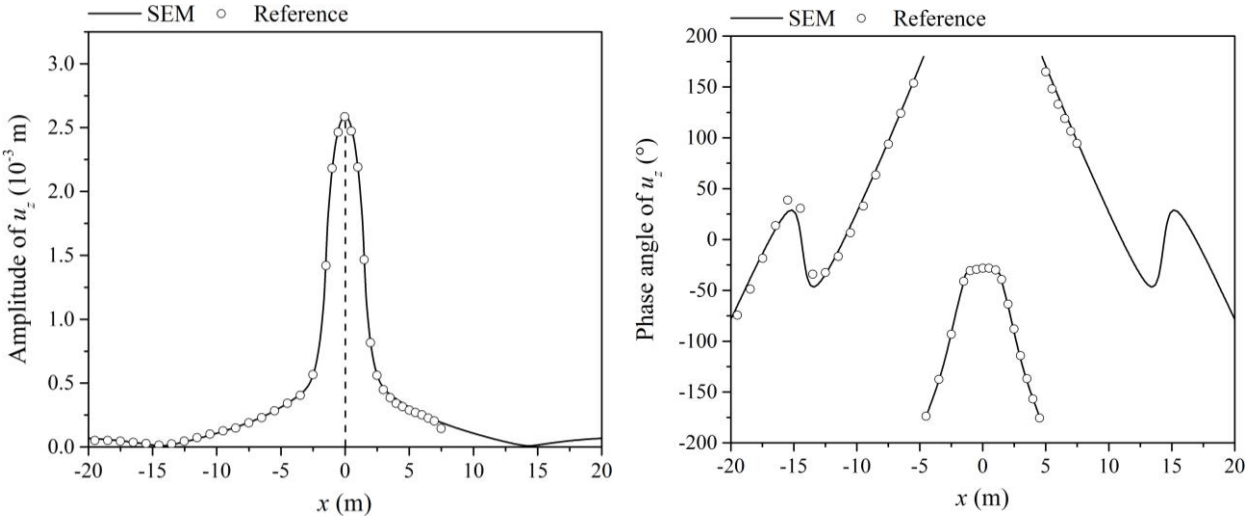

(b)

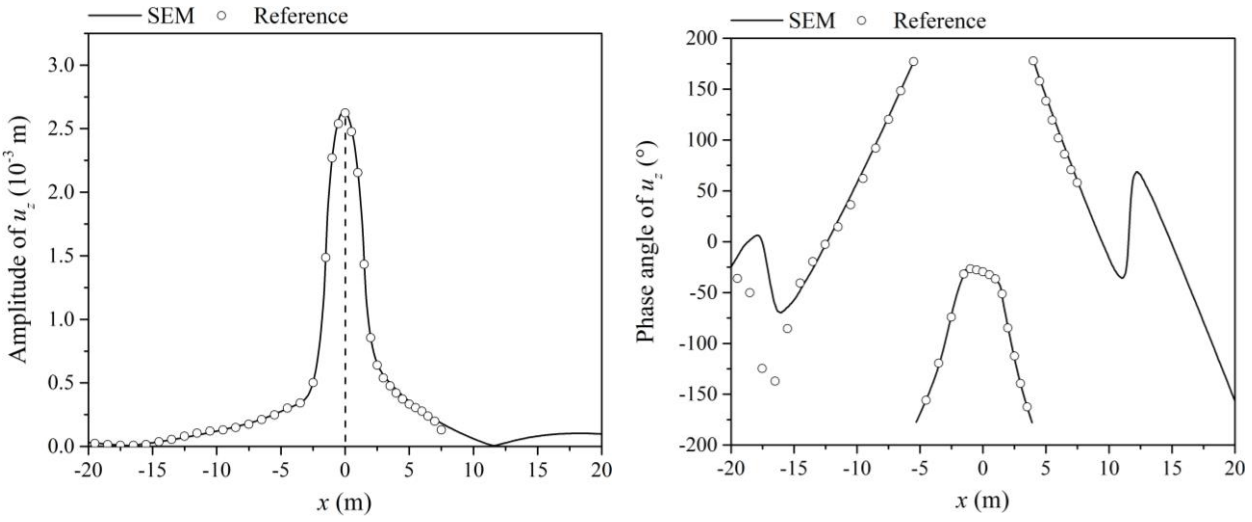

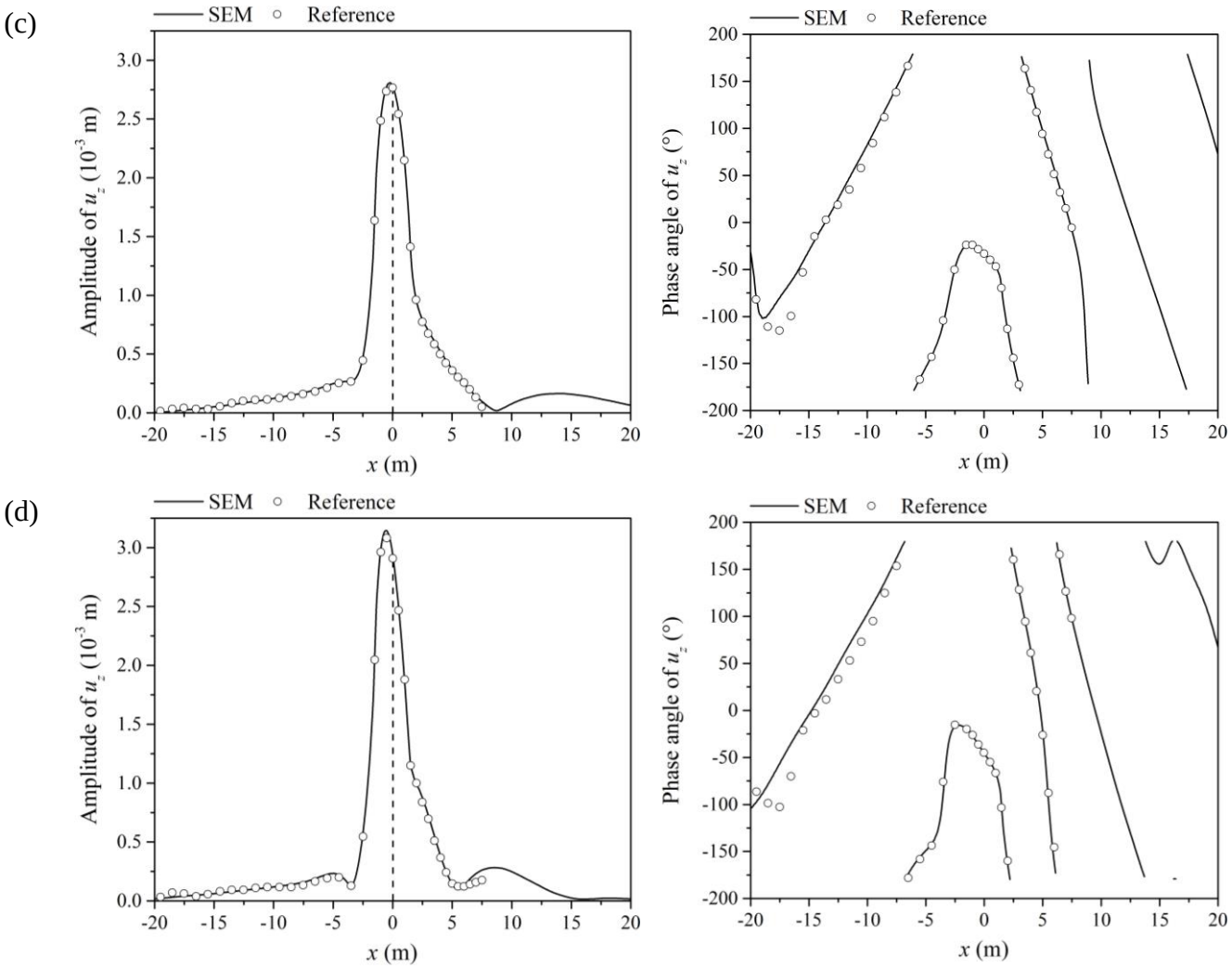

Figure 5. Comparison of u_z for points along the x-axis on the layered system surface calculated by different methods at different moving velocities: (a) c = 0 m/s, (b) c = 25 m/s, (c) c = 50 m/s, and (d) c = 75 m/s.

The results shown in this section indicate that the displacement amplitude curve decreases more rapidly in front of the loading area, which is more obvious at higher velocities. The reason of this phenomenon is the uneven wave field distribution in the vicinity of the loading area caused by the Doppler effect (Lefeuve-Mesgouez et al., 2002). The wavelengths of the waves in front of the loading area are shorter while the wavelengths of the waves behind the loading area are longer. Hence, the moving load has a smaller influencing area in front of the load than behind it.

3.3. Comparison with field measurements

LINTRACK was used to measure the strains of an asphalt pavement structure which was designed for a heavily loaded motorway. The first layer is porous asphalt

concrete (PAC), the second layer is newly applied stone asphalt concrete (New STAC), the third layer is old STAC, the fourth layer is asphalt granulate cement (AGRAC), and the foundation is a thick and well-compacted sand subgrade. The parameter values of the tested pavement structure are shown in Table 3. Strain gauges were installed at the bottom of the first layer in the longitudinal direction (direction of movement). During the measurements, the LINTRACK belt moved straight over the built-in strain gauges at a constant speed of 2.5 m/s. A constant force was applied on the tire, while the tire pressure was maintained to be 900 kPa.

Table 3 Parameter values of the tested pavement structure

Layers	ρ	E	v	η	h
	kg/m^3	MPa	-	-	m
PAC	2090	5525	0.25	0.1	0.05
New STAC	2395	7225	0.25	0.1	0.06
STAC	2395	8500	0.25	0.1	0.17
AGRAC	2141	5400	0.25	0.2	0.25
Subgrade	1733	126	0.4	0.4	Infinite

The maximum longitudinal strains of the pavement structure calculated by the presented model are compared with those measured by the strain gauges. The results are shown in Table 4, which indicates a good match between the simulated and measured data, and thus further proves the accuracy of the presented model.

Table 4 Comparison between the simulated and measured maximum longitudinal strains

Cases	Forces	Maximum longitudinal strains (10^{-6})	
	kN	Simulated	Measured
1	20	19	19
2	25	21	21
3	30	22	22
4	35	24	23
5	40	25	24
6	45	27	26

4. Response analysis of a pavement structure

This section focuses on a specific pavement structure subjected to a surface moving load, and the parameter sensitivity analysis and stress analysis are conducted. The reference loading conditions are described as follows:

- A uniformly distributed harmonically varying load moves in the positive direction of the *x*-axis on the surface of a pavement structure;
- The moving velocity is c = 25 m/s (90 km/h);
- The loading frequency is $f_0 = 20$ Hz;
- The loading amplitude is $p_0 = 550$ kPa;
- The dimensions of loading area are $2x_0 = 2y_0 = 0.2683$ m;
- The dimensions of the space window are $2X_0 = 2Y_0 = 400$ m.

The total force applied on the surface is about 39.6 kN, which is comparable to the actual traffic load. The detailed reference parameter values of a pavement structure are shown in Table 5.

Table 5 Reference parameter values of a pavement structure

Layers	ρ	E	v	η	h
	kg/m^3	MPa	-	-	m
1	2400	1000	0.35	0.1	0.1
2	2000	500	0.35	0.1	0.3
3	1600	60	0.35	0.1	Infinite

4.1. Parameter sensitivity analysis

By using single factor analysis, the sensitivity of the displacement amplitude curve along the *x*-axis on the pavement surface to different parameters is investigated. The results are shown in Figure 6, in which the response of the reference structural configuration to the reference loading is shown in solid line. It is assumed that all the layers in the pavement structure have the same Poisson's ratio and loss factor.

4.1.1. Sensitivity to moving velocity

The displacement amplitude curves along the *x*-axis on the pavement surface caused by a load moving at different velocities (c = 5, 25, and 45 m/s) are shown in Figure 6(a). The effect of the moving velocity is similar to that observed in the previous section. However, for a realistic pavement structure, the curves are very smooth because of the relatively high structural stiffness, and the Doppler effect is not as significant as that observed for the layered soil systems. In addition, within the range of analyses, the maximum of the displacement amplitude curve is slightly affected by the moving velocity.

4.1.2. Sensitivity to loading frequency

The displacement amplitude curves along the *x*-axis on the pavement surface caused by a moving load with different loading frequencies (f_0 = 10, 20, and 30 Hz) are shown in Figure 6(b). The vertical displacement amplitudes of the surface points along the moving direction are smaller if the loading frequency is higher, which might be the result of the damping mechanism playing a more pronounced role.

4.1.3. Sensitivity to loading area

The displacement amplitude curves along the *x*-axis on the pavement surface caused by a moving load with different loading areas (s_0 = 0.036, 0.072, and 0.108 m^2) but the same amplitude of the total force (39.6 kN) are shown in Figure 6(c). It can be seen that the maximum of the curve is higher if the loading area is smaller, which is caused by the increase of the loading pressure. However, the differences appear only in the close vicinity of the loading area, the displacement amplitudes of points outside are almost identical. Therefore, if the applied force is the same, the effect of the loading area is localised in the close vicinity of the load.

4.1.4. Sensitivity to loss factor

The surface displacement amplitude curves along the *x*-axis for pavement structures with different loss factors (η = 0.1, 0.2, and 0.3) under reference loading conditions are shown in Figure 6(d). It can be seen that the curve is slightly lower if the loss factor is higher. More energy is dissipated for a system with higher loss factor, which results in smaller displacements.

4.1.5. Sensitivity to Poisson's ratio

The surface displacement amplitude curves along the *x*-axis for pavement structures with different Poisson's ratios (ν = 0.25, 0.35, and 0.45) under reference loading conditions are shown in Figure 6(e). The maximum of the curve is slightly smaller if the Poisson's ratio is larger, while the displacement amplitudes of points outside the loading area are almost unaffected.

(a)

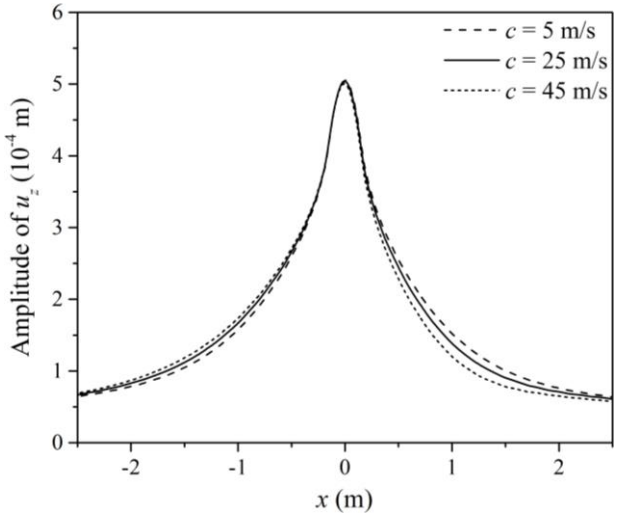

(b)

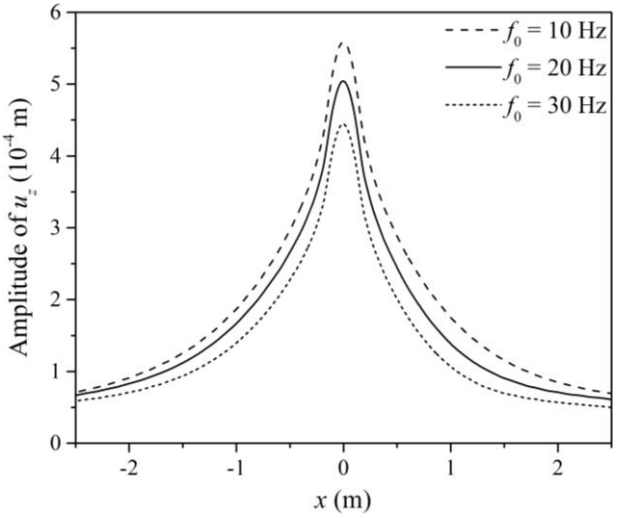

(c)

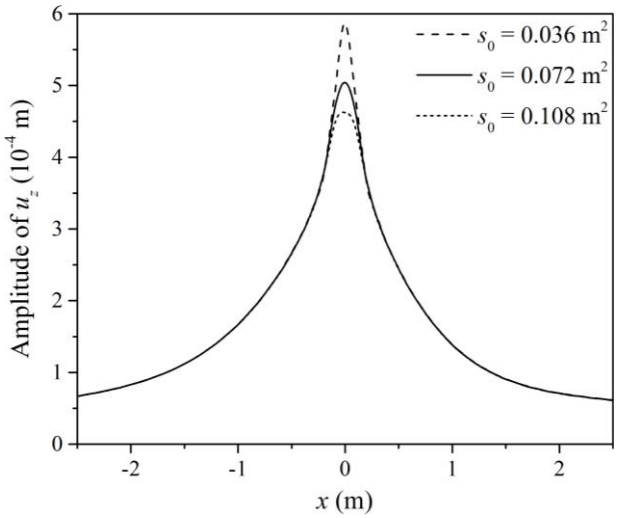

(d)

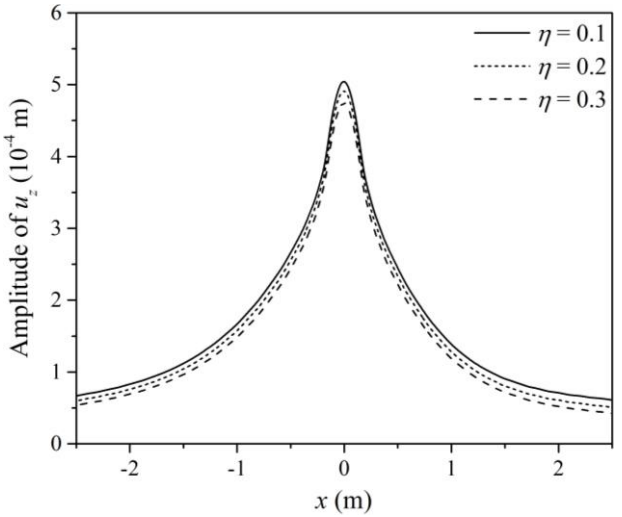

(e)

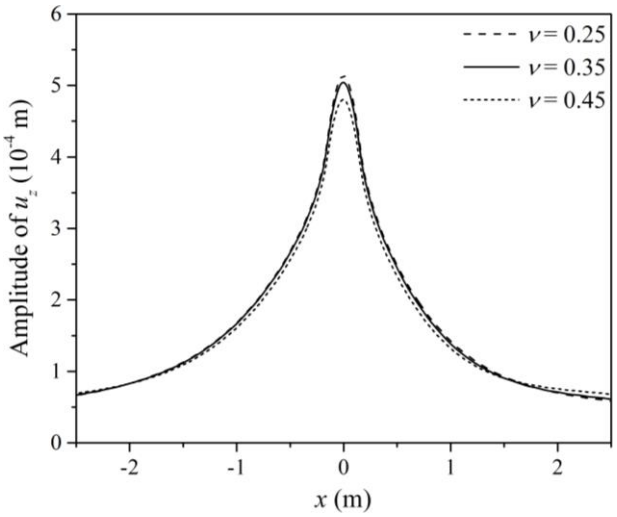

Figure 6. Sensitivity of the amplitudes of u_z for points along the x-axis on the pavement surface to different parameters: (a) Moving velocity, (b) Loading frequency, (c) Loading area, (d) Loss factor, and (e) Poisson's ratio.

It should be highlighted that Figure 6 only shows the amplitudes of u_z for points along the x-axis on the surface. In reality, all quantities at all points are harmonically varying, as shown in equation (76). Furthermore, for a pavement structure with the reference structural configuration subjected to the reference loading condition, the profiles of u_z for points along different axes on the pavement surface for t = 0 are shown in Figure 7. The results show that the profile of u_z is asymmetric along the x-axis while symmetric along the y-axis, which means the Doppler effect appears only in the moving direction.

(a)

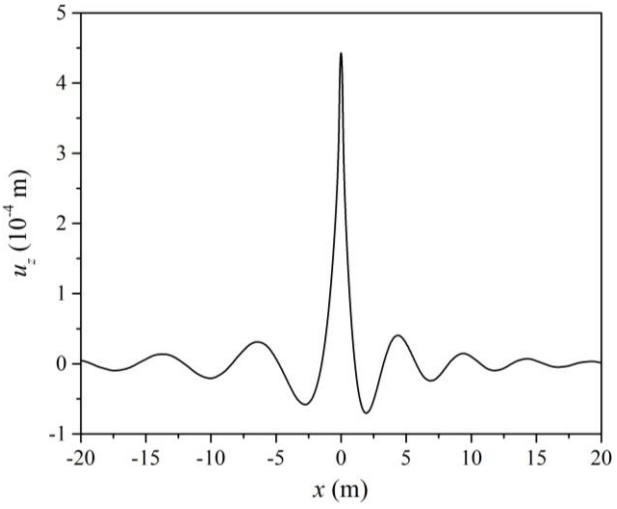

(b)

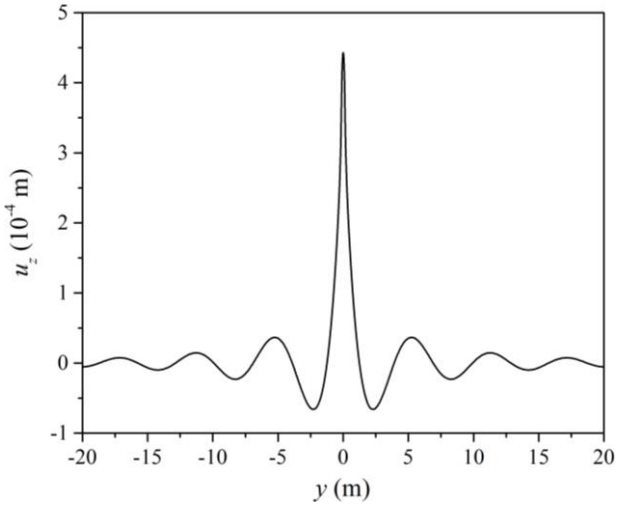

Figure 7. Profiles of u_z for points along different axes on the pavement surface for t = 0: (a) x-axis and (b) y-axis.

4.2. Stress analysis

For a pavement structure with the reference loading and structural configuration, the stresses of points along the *x*-axis at depth 0.1 m are simulated by the presented model. The results for $t = 0$ are shown in Figure 8, which indicates that the points under the loading area are most critical. For these points, the maximum stress component is σ_{zz}, which is followed by σ_{xx}, σ_{zx}, and σ_{yy}. In addition, the stress components of σ_{xy} and σ_{yz} are negligibly small. The stresses calculated by the presented model could be used for pavement structural design to ensure its durability.

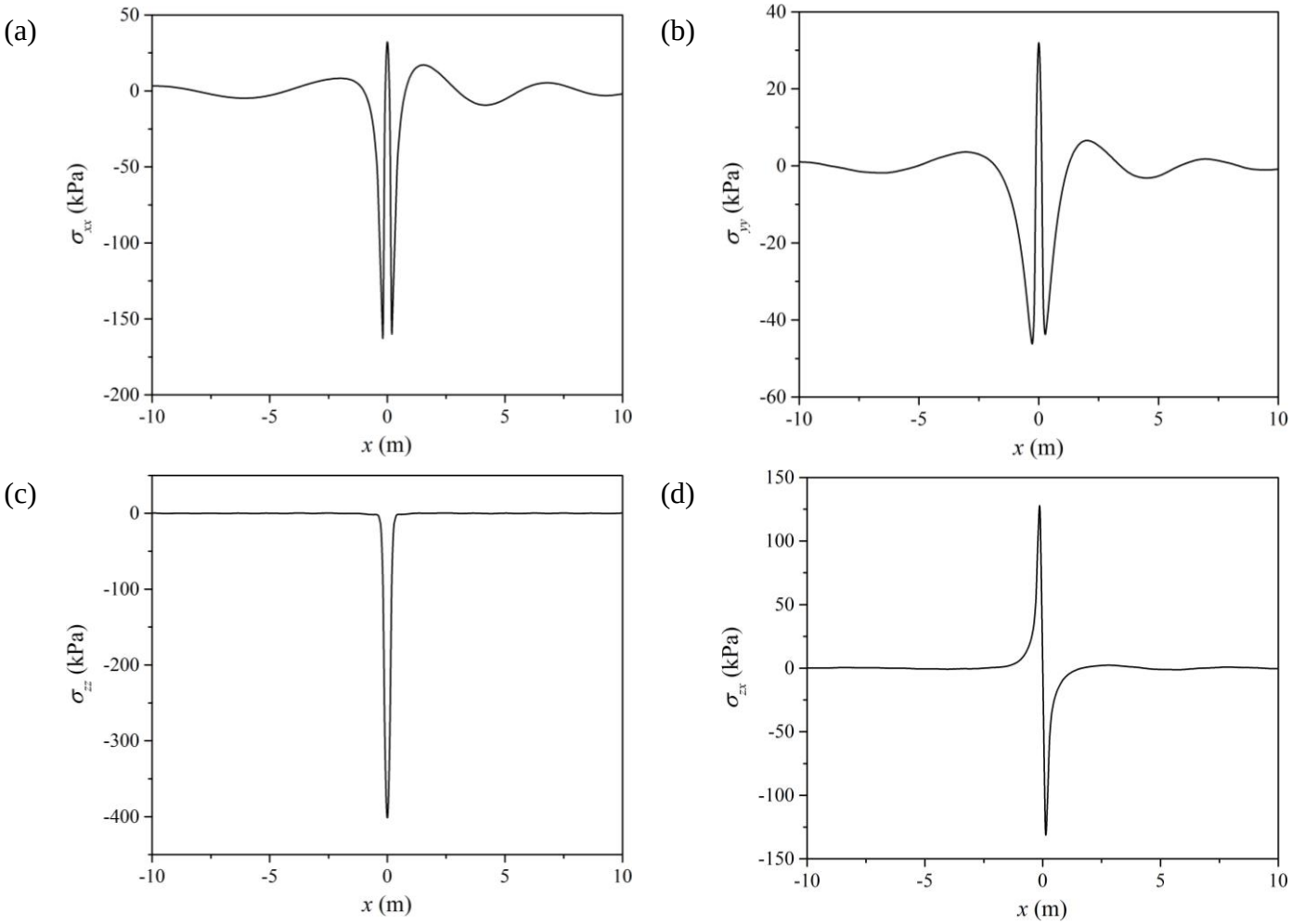

Figure 8. Stresses of points along the *x*-axis at depth 0.1 m for $t = 0$: (a) σ_{xx}, (b) σ_{yy}, (c) σ_{zz}, and (d) σ_{zx}.

5. Conclusions and recommendations

This paper proposes a SEM-based model which can be used to analyse the

dynamic response of layered systems caused by a moving load. Based on the discussion shown in this paper, the following conclusions can be drawn:

(1) The proposed model is robust for the dynamic analysis of layered systems under a moving load, and this model is a potential tool for pavement structural design.

(2) The displacement amplitude curves and phase angle curves along the moving direction are asymmetric when the load moves, and this asymmetry is more dominant if the moving velocity is higher. The reason of this phenomenon is the inhomogeneous wave field distribution caused by the Doppler effect. However, the moving velocity only has slight effect on the maximum of the surface displacement amplitude curve within the scope of analysis.

(3) The surface displacement amplitude curve will be lower if the loading frequency is higher or the loss factor is bigger, and the effect of the former is more dominant.

(4) If the amplitude of the applied total force is constant, the loading area only has influence on the displacement amplitudes of points in the close vicinity of the load.

(5) The Poisson's ratio has slight effect on the maximum of the displacement amplitude curve, and it almost does not affect the displacement amplitudes of points outside the loading area.

(6) The presented model is a promising parameter back-calculation engine for pavement quality evaluation.

This paper proposed a 3D dynamic model for elastic layered systems under a moving load, which is combined with a hysteretic damping model to analyse the response of a pavement structure caused by a moving harmonic load. In order to consider the frequency-dependent viscous effect in pavement structures, it is recommended to use more suitable damping models.

Conflict of interest

None.

Acknowledgements

This work is financially supported by the China Scholarship Council (No. 201608230114). The first author is grateful to the discussions with Mingjuan Zhao, who is a PhD candidate of the Department of Engineering Structures, Faculty of Civil Engineering and Geosciences, Delft University of Technology.

Appendix A

In the moving coordinate system, the Navier's equation has the following form:

$$(\lambda+\mu)\nabla\nabla\cdot\underline{\mathbf{u}}+\mu\nabla^2\underline{\mathbf{u}}=\rho\left(\frac{\partial}{\partial t}-\underline{\mathbf{c}}\cdot\frac{\partial}{\partial\underline{\mathbf{x}}}\right)^2\underline{\mathbf{u}} \tag{A1.1}$$

The Helmholtz decomposition of the displacement field is expressed as:

$$\underline{\mathbf{u}}=\nabla\phi+\nabla\times\underline{\boldsymbol{\psi}} \tag{A1.2}$$

By substituting equation (A1.2) into equation (A1.1), considering the identities of $\nabla\cdot\nabla\phi=\nabla^2\phi$ and $\nabla\cdot\nabla\times\underline{\boldsymbol{\psi}}=0$, and interchanging the order of the operators gives:

$$\nabla\left[(\lambda+2\mu)\nabla^2\phi-\rho\left(\frac{\partial}{\partial t}-\underline{\mathbf{c}}\cdot\frac{\partial}{\partial\underline{\mathbf{x}}}\right)^2\phi\right]+\nabla\times\left[\mu\nabla^2\underline{\boldsymbol{\psi}}-\rho\left(\frac{\partial}{\partial t}-\underline{\mathbf{c}}\cdot\frac{\partial}{\partial\underline{\mathbf{x}}}\right)^2\underline{\boldsymbol{\psi}}\right]=\underline{\mathbf{0}} \tag{A1.3}$$

This equation will be satisfied if the terms in the square brackets vanish, hence:

$$\nabla^2\phi-\frac{1}{c_{\mathrm{P}}^2}\left(\frac{\partial}{\partial t}-\underline{\mathbf{c}}\cdot\frac{\partial}{\partial\underline{\mathbf{x}}}\right)^2\phi=0 \tag{A1.4}$$

$$\nabla^2\underline{\boldsymbol{\psi}}-\frac{1}{c_{\mathrm{S}}^2}\left(\frac{\partial}{\partial t}-\underline{\mathbf{c}}\cdot\frac{\partial}{\partial\underline{\mathbf{x}}}\right)^2\underline{\boldsymbol{\psi}}=\underline{\mathbf{0}} \tag{A1.5}$$

with $c_{\mathrm{P}}=\sqrt{(\lambda+2\mu)/\rho}$ and $c_{\mathrm{S}}=\sqrt{\mu/\rho}$.

If the velocity vector has the form of $\underline{\mathbf{c}}=\begin{bmatrix}c & 0 & 0\end{bmatrix}^{\mathrm{T}}$, then the equations (A1.4) and (A1.5) become:

$$\nabla^2\phi-\frac{1}{c_{\mathrm{P}}^2}\left(\frac{\partial}{\partial t}-c\frac{\partial}{\partial x}\right)^2\phi=0 \tag{A1.6}$$

$$\nabla^2\underline{\boldsymbol{\psi}}-\frac{1}{c_{\mathrm{S}}^2}\left(\frac{\partial}{\partial t}-c\frac{\partial}{\partial x}\right)^2\underline{\boldsymbol{\psi}}=\underline{\mathbf{0}} \tag{A1.7}$$

Appendix B

The element stiffness matrix $\hat{\underline{\underline{\mathbf{k}}}}^{\mathrm{e}}$ of the layer spectral element can be expressed as follows:

$$\hat{\underline{\underline{\mathbf{k}}}}^{\mathrm{e}}=\begin{bmatrix}\hat{k}_{11}^{\mathrm{e}} & \hat{k}_{12}^{\mathrm{e}} & \hat{k}_{13}^{\mathrm{e}} & \hat{k}_{14}^{\mathrm{e}} & \hat{k}_{15}^{\mathrm{e}} & \hat{k}_{16}^{\mathrm{e}}\\ \hat{k}_{12}^{\mathrm{e}} & \hat{k}_{22}^{\mathrm{e}} & \hat{k}_{23}^{\mathrm{e}} & \hat{k}_{15}^{\mathrm{e}} & \hat{k}_{25}^{\mathrm{e}} & \hat{k}_{26}^{\mathrm{e}}\\ -\hat{k}_{13}^{\mathrm{e}} & -\hat{k}_{23}^{\mathrm{e}} & \hat{k}_{33}^{\mathrm{e}} & \hat{k}_{16}^{\mathrm{e}} & \hat{k}_{26}^{\mathrm{e}} & \hat{k}_{36}^{\mathrm{e}}\\ \hat{k}_{14}^{\mathrm{e}} & \hat{k}_{15}^{\mathrm{e}} & -\hat{k}_{16}^{\mathrm{e}} & \hat{k}_{11}^{\mathrm{e}} & \hat{k}_{12}^{\mathrm{e}} & -\hat{k}_{13}^{\mathrm{e}}\\ \hat{k}_{15}^{\mathrm{e}} & \hat{k}_{25}^{\mathrm{e}} & -\hat{k}_{26}^{\mathrm{e}} & \hat{k}_{12}^{\mathrm{e}} & \hat{k}_{22}^{\mathrm{e}} & -\hat{k}_{23}^{\mathrm{e}}\\ -\hat{k}_{16}^{\mathrm{e}} & -\hat{k}_{26}^{\mathrm{e}} & \hat{k}_{36}^{\mathrm{e}} & \hat{k}_{13}^{\mathrm{e}} & \hat{k}_{23}^{\mathrm{e}} & \hat{k}_{33}^{\mathrm{e}}\end{bmatrix}$$

in which

$$\hat{k}_{11}^{\mathrm{e}}=\frac{\mathrm{i}\mu}{\Delta}\begin{Bmatrix}2k_{\mathrm{Pz}}\left[k_x^4+k_x^2k_y^2+\left(k_x^2-2k_y^2\right)k_{\mathrm{Sz}}^2\right]\left[e^{-2\mathrm{i}\left(k_{\mathrm{Pz}}+k_{\mathrm{Sz}}\right)h}+e^{-2\mathrm{i}k_{\mathrm{Sz}}h}\right]-\left(k_x^2+k_y^2+k_{\mathrm{Pz}}k_{\mathrm{Sz}}\right)\left[\left(k_x^2+k_{\mathrm{Sz}}^2\right)k_{\mathrm{Pz}}+k_y^2k_{\mathrm{Sz}}\right]\left[e^{-2\mathrm{i}\left(k_{\mathrm{Pz}}+2k_{\mathrm{Sz}}\right)h}+1\right]\\ +8k_y^2k_{\mathrm{Pz}}k_{\mathrm{Sz}}^2\left[e^{-\mathrm{i}\left(k_{\mathrm{Pz}}+k_{\mathrm{Sz}}\right)h}+e^{-\mathrm{i}\left(k_{\mathrm{Pz}}+3k_{\mathrm{Sz}}\right)h}\right]-\left(k_x^2+k_y^2-k_{\mathrm{Pz}}k_{\mathrm{Sz}}\right)\left[\left(k_x^2+k_{\mathrm{Sz}}^2\right)k_{\mathrm{Pz}}-k_y^2k_{\mathrm{Sz}}\right]\left(e^{-2\mathrm{i}k_{\mathrm{Pz}}h}+e^{-4\mathrm{i}k_{\mathrm{Sz}}h}\right)\end{Bmatrix}$$

$$\hat{k}_{12}^{\mathrm{e}}=\frac{\mathrm{i}\mu k_xk_y}{\Delta}\begin{Bmatrix}2k_{\mathrm{Pz}}\left(k_x^2+k_y^2+3k_{\mathrm{Sz}}^2\right)\left[e^{-2\mathrm{i}\left(k_{\mathrm{Pz}}+k_{\mathrm{Sz}}\right)h}+e^{-2\mathrm{i}k_{\mathrm{Sz}}h}\right]-\left(k_x^2+k_y^2+k_{\mathrm{Pz}}k_{\mathrm{Sz}}\right)\left(k_{\mathrm{Pz}}-k_{\mathrm{Sz}}\right)\left[e^{-2\mathrm{i}\left(k_{\mathrm{Pz}}+2k_{\mathrm{Sz}}\right)h}+1\right]\\ -8k_{\mathrm{Pz}}k_{\mathrm{Sz}}^2\left[e^{-\mathrm{i}\left(k_{\mathrm{Pz}}+k_{\mathrm{Sz}}\right)h}+e^{-\mathrm{i}\left(k_{\mathrm{Pz}}+3k_{\mathrm{Sz}}\right)h}\right]-\left(k_x^2+k_y^2-k_{\mathrm{Pz}}k_{\mathrm{Sz}}\right)\left(k_{\mathrm{Pz}}+k_{\mathrm{Sz}}\right)\left(e^{-2\mathrm{i}k_{\mathrm{Pz}}h}+e^{-4\mathrm{i}k_{\mathrm{Sz}}h}\right)\end{Bmatrix}$$

$$\hat{k}_{13}^{\mathrm{e}}=-\frac{\mathrm{i}\mu k_x}{\Delta}\begin{Bmatrix}2\left[\left(k_x^2+k_y^2\right)^2-\left(k_x^2+k_y^2-2k_{\mathrm{Pz}}^2\right)k_{\mathrm{Sz}}^2\right]\left[e^{-2\mathrm{i}\left(k_{\mathrm{Pz}}+k_{\mathrm{Sz}}\right)h}-e^{-2\mathrm{i}k_{\mathrm{Sz}}h}\right]-\left(k_x^2+k_y^2+k_{\mathrm{Pz}}k_{\mathrm{Sz}}\right)\left(k_x^2+k_y^2+2k_{\mathrm{Pz}}k_{\mathrm{Sz}}-k_{\mathrm{Sz}}^2\right)\left[e^{-2\mathrm{i}\left(k_{\mathrm{Pz}}+2k_{\mathrm{Sz}}\right)h}-1\right]\\ +4k_{\mathrm{Pz}}k_{\mathrm{Sz}}\left[3\left(k_x^2+k_y^2\right)-k_{\mathrm{Sz}}^2\right]\left[e^{-\mathrm{i}\left(k_{\mathrm{Pz}}+3k_{\mathrm{Sz}}\right)h}-e^{-\mathrm{i}\left(k_{\mathrm{Pz}}+k_{\mathrm{Sz}}\right)h}\right]-\left(k_x^2+k_y^2-k_{\mathrm{Pz}}k_{\mathrm{Sz}}\right)\left(k_x^2+k_y^2-2k_{\mathrm{Pz}}k_{\mathrm{Sz}}-k_{\mathrm{Sz}}^2\right)\left(e^{-2\mathrm{i}k_{\mathrm{Pz}}h}-e^{-4\mathrm{i}k_{\mathrm{Sz}}h}\right)\end{Bmatrix}$$

$$\hat{k}_{14}^{\mathrm{e}}=-\frac{2\mathrm{i}\mu}{\Delta}\begin{Bmatrix}2k_{\mathrm{Pz}}\left[k_x^4+k_x^2k_y^2+\left(k_x^2+4k_y^2\right)k_{\mathrm{Sz}}^2\right]e^{-\mathrm{i}\left(k_{\mathrm{Pz}}+2k_{\mathrm{Sz}}\right)h}-k_{\mathrm{Sz}}\left(k_y^4+k_x^2k_y^2+k_x^2k_{\mathrm{Pz}}^2+2k_y^2k_{\mathrm{Pz}}k_{\mathrm{Sz}}+k_{\mathrm{Pz}}^2k_{\mathrm{Sz}}^2\right)\left[e^{-\mathrm{i}\left(2k_{\mathrm{Pz}}+3k_{\mathrm{Sz}}\right)h}+e^{-\mathrm{i}k_{\mathrm{Sz}}h}\right]\\ -k_x^2k_{\mathrm{Pz}}\left(k_x^2+k_y^2+k_{\mathrm{Sz}}^2\right)\left[e^{-\mathrm{i}k_{\mathrm{Pz}}h}+e^{-\mathrm{i}\left(k_{\mathrm{Pz}}+4k_{\mathrm{Sz}}\right)h}\right]+k_{\mathrm{Sz}}\left(k_y^4+k_x^2k_y^2+k_x^2k_{\mathrm{Pz}}^2-2k_y^2k_{\mathrm{Pz}}k_{\mathrm{Sz}}+k_{\mathrm{Pz}}^2k_{\mathrm{Sz}}^2\right)\left[e^{-\mathrm{i}\left(2k_{\mathrm{Pz}}+k_{\mathrm{Sz}}\right)h}+e^{-3\mathrm{i}k_{\mathrm{Sz}}h}\right]\end{Bmatrix}$$

$$\hat{k}_{15}^{\mathrm{e}}=-\frac{2\mathrm{i}\mu k_xk_y}{\Delta}\begin{Bmatrix}k_{\mathrm{Sz}}\left(k_x^2+k_y^2-k_{\mathrm{Pz}}^2+2k_{\mathrm{Pz}}k_{\mathrm{Sz}}\right)\left[e^{-\mathrm{i}\left(2k_{\mathrm{Pz}}+3k_{\mathrm{Sz}}\right)h}+e^{-\mathrm{i}k_{\mathrm{Sz}}h}\right]-k_{\mathrm{Pz}}\left(k_x^2+k_y^2+k_{\mathrm{Sz}}^2\right)\left[e^{-\mathrm{i}k_{\mathrm{Pz}}h}+e^{-\mathrm{i}\left(k_{\mathrm{Pz}}+4k_{\mathrm{Sz}}\right)h}\right]\\ -k_{\mathrm{Sz}}\left(k_x^2+k_y^2-k_{\mathrm{Pz}}^2-2k_{\mathrm{Pz}}k_{\mathrm{Sz}}\right)\left[e^{-\mathrm{i}\left(2k_{\mathrm{Pz}}+k_{\mathrm{Sz}}\right)h}+e^{-3\mathrm{i}k_{\mathrm{Sz}}h}\right]+2k_{\mathrm{Pz}}\left(k_x^2+k_y^2-3k_{\mathrm{Sz}}^2\right)e^{-\mathrm{i}\left(k_{\mathrm{Pz}}+2k_{\mathrm{Sz}}\right)h}\end{Bmatrix}$$

$$\hat{k}_{16}^{\mathrm{e}}=-\frac{2\mathrm{i}\mu k_xk_{\mathrm{Pz}}k_{\mathrm{Sz}}}{\Delta}\left(k_x^2+k_y^2+k_{\mathrm{Sz}}^2\right)\left[e^{-\mathrm{i}k_{\mathrm{Pz}}h}-e^{-\mathrm{i}\left(k_{\mathrm{Pz}}+4k_{\mathrm{Sz}}\right)h}-e^{-\mathrm{i}\left(2k_{\mathrm{Pz}}+k_{\mathrm{Sz}}\right)h}+e^{-\mathrm{i}\left(2k_{\mathrm{Pz}}+3k_{\mathrm{Sz}}\right)h}-e^{-\mathrm{i}k_{\mathrm{Sz}}h}+e^{-3\mathrm{i}k_{\mathrm{Sz}}h}\right]$$

$$\hat{k}_{22}^{\mathrm{e}}=\frac{\mathrm{i}\mu}{\Delta}\begin{Bmatrix}2k_{\mathrm{Pz}}\left[k_y^4+k_x^2k_y^2-\left(2k_x^2-k_y^2\right)k_{\mathrm{Sz}}^2\right]\left[e^{-2\mathrm{i}\left(k_{\mathrm{Pz}}+k_{\mathrm{Sz}}\right)h}+e^{-2\mathrm{i}k_{\mathrm{Sz}}h}\right]-\left(k_x^2+k_y^2+k_{\mathrm{Pz}}k_{\mathrm{Sz}}\right)\left[\left(k_y^2+k_{\mathrm{Sz}}^2\right)k_{\mathrm{Pz}}+k_x^2k_{\mathrm{Sz}}\right]\left[e^{-2\mathrm{i}\left(k_{\mathrm{Pz}}+2k_{\mathrm{Sz}}\right)h}+1\right]\\ +8k_x^2k_{\mathrm{Pz}}k_{\mathrm{Sz}}^2\left[e^{-\mathrm{i}\left(k_{\mathrm{Pz}}+k_{\mathrm{Sz}}\right)h}+e^{-\mathrm{i}\left(k_{\mathrm{Pz}}+3k_{\mathrm{Sz}}\right)h}\right]-\left(k_x^2+k_y^2-k_{\mathrm{Pz}}k_{\mathrm{Sz}}\right)\left[\left(k_y^2+k_{\mathrm{Sz}}^2\right)k_{\mathrm{Pz}}-k_x^2k_{\mathrm{Sz}}\right]\left(e^{-2\mathrm{i}k_{\mathrm{Pz}}h}+e^{-4\mathrm{i}k_{\mathrm{Sz}}h}\right)\end{Bmatrix}$$

$$\hat{k}_{23}^{\mathrm{e}}=-\frac{\mathrm{i}\mu k_y}{\Delta}\begin{Bmatrix}2\left[\left(k_x^2+k_y^2\right)^2-\left(k_x^2+k_y^2-2k_{\mathrm{Pz}}^2\right)k_{\mathrm{Sz}}^2\right]\left[e^{-2\mathrm{i}\left(k_{\mathrm{Pz}}+k_{\mathrm{Sz}}\right)h}-e^{-2\mathrm{i}k_{\mathrm{Sz}}h}\right]-\left(k_x^2+k_y^2+k_{\mathrm{Pz}}k_{\mathrm{Sz}}\right)\left(k_x^2+k_y^2+2k_{\mathrm{Pz}}k_{\mathrm{Sz}}-k_{\mathrm{Sz}}^2\right)\left[e^{-2\mathrm{i}\left(k_{\mathrm{Pz}}+2k_{\mathrm{Sz}}\right)h}-1\right]\\ -4k_{\mathrm{Pz}}k_{\mathrm{Sz}}\left[3\left(k_x^2+k_y^2\right)-k_{\mathrm{Sz}}^2\right]\left[e^{-\mathrm{i}\left(k_{\mathrm{Pz}}+k_{\mathrm{Sz}}\right)h}-e^{-\mathrm{i}\left(k_{\mathrm{Pz}}+3k_{\mathrm{Sz}}\right)h}\right]-\left(k_x^2+k_y^2-k_{\mathrm{Pz}}k_{\mathrm{Sz}}\right)\left(k_x^2+k_y^2-2k_{\mathrm{Pz}}k_{\mathrm{Sz}}-k_{\mathrm{Sz}}^2\right)\left(e^{-2\mathrm{i}k_{\mathrm{Pz}}h}-e^{-4\mathrm{i}k_{\mathrm{Sz}}h}\right)\end{Bmatrix}$$

$$\hat{k}_{25}^{\mathrm{e}}=-\frac{2\mathrm{i}\mu}{\Delta}\begin{Bmatrix}2k_{\mathrm{Pz}}\left[k_y^4+k_x^2k_y^2+\left(4k_x^2+k_y^2\right)k_{\mathrm{Sz}}^2\right]e^{-\mathrm{i}\left(k_{\mathrm{Pz}}+2k_{\mathrm{Sz}}\right)h}-k_{\mathrm{Sz}}\left(k_x^4+k_x^2k_y^2+2k_x^2k_{\mathrm{Pz}}k_{\mathrm{Sz}}+k_y^2k_{\mathrm{Pz}}^2+k_{\mathrm{Pz}}^2k_{\mathrm{Sz}}^2\right)\left[e^{-\mathrm{i}\left(2k_{\mathrm{Pz}}+3k_{\mathrm{Sz}}\right)h}+e^{-\mathrm{i}k_{\mathrm{Sz}}h}\right]\\ -k_y^2k_{\mathrm{Pz}}\left(k_x^2+k_y^2+k_{\mathrm{Sz}}^2\right)\left[e^{-\mathrm{i}k_{\mathrm{Pz}}h}+e^{-\mathrm{i}\left(k_{\mathrm{Pz}}+4k_{\mathrm{Sz}}\right)h}\right]+k_{\mathrm{Sz}}\left(k_x^4+k_x^2k_y^2-2k_x^2k_{\mathrm{Pz}}k_{\mathrm{Sz}}+k_y^2k_{\mathrm{Pz}}^2+k_{\mathrm{Pz}}^2k_{\mathrm{Sz}}^2\right)\left[e^{-\mathrm{i}\left(2k_{\mathrm{Pz}}+k_{\mathrm{Sz}}\right)h}+e^{-3\mathrm{i}k_{\mathrm{Sz}}h}\right]\end{Bmatrix}$$

733 $$\hat{k}^{\mathrm{e}}_{26} = -\frac{2\mathrm{i}\mu k_y k_{\mathrm{Pz}} k_{\mathrm{Sz}}}{\Delta}\left(k_x^2 + k_y^2 + k_{\mathrm{Sz}}^2\right)\left[e^{-\mathrm{i}k_{\mathrm{Pz}}h} - e^{-\mathrm{i}\left(k_{\mathrm{Pz}}+4k_{\mathrm{Sz}}\right)h} - e^{-\mathrm{i}\left(2k_{\mathrm{Pz}}+k_{\mathrm{Sz}}\right)h} + e^{-\mathrm{i}\left(2k_{\mathrm{Pz}}+3k_{\mathrm{Sz}}\right)h} - e^{-\mathrm{i}k_{\mathrm{Sz}}h} + e^{-3\mathrm{i}k_{\mathrm{Sz}}h}\right]$$

734 $$\hat{k}^{\mathrm{e}}_{33} = \frac{\mathrm{i}\mu k_{\mathrm{Sz}}}{\Delta}\left(k_x^2 + k_y^2 + k_{\mathrm{Sz}}^2\right)\begin{Bmatrix}\left(k_x^2 + k_y^2\right)\left[e^{-2\mathrm{i}k_{\mathrm{Pz}}h} - e^{-2\mathrm{i}\left(k_{\mathrm{Pz}}+2k_{\mathrm{Sz}}\right)h} + e^{-4\mathrm{i}k_{\mathrm{Sz}}h} - 1\right] \\ -k_{\mathrm{Pz}}k_{\mathrm{Sz}}\left[e^{-2\mathrm{i}k_{\mathrm{Pz}}h} - 2e^{-2\mathrm{i}\left(k_{\mathrm{Pz}}+k_{\mathrm{Sz}}\right)h} + e^{-2\mathrm{i}\left(k_{\mathrm{Pz}}+2k_{\mathrm{Sz}}\right)h} - 2e^{-2\mathrm{i}k_{\mathrm{Sz}}h} + e^{-4\mathrm{i}k_{\mathrm{Sz}}h} + 1\right]\end{Bmatrix}$$

735 $$\hat{k}^{\mathrm{e}}_{36} = -\frac{2\mathrm{i}\mu k_{\mathrm{Sz}}}{\Delta}\left(k_x^2 + k_y^2 + k_{\mathrm{Sz}}^2\right)\begin{Bmatrix}\left(k_x^2 + k_y^2\right)\left[e^{-\mathrm{i}\left(2k_{\mathrm{Pz}}+k_{\mathrm{Sz}}\right)h} - e^{-\mathrm{i}\left(2k_{\mathrm{Pz}}+3k_{\mathrm{Sz}}\right)h} - e^{-\mathrm{i}k_{\mathrm{Sz}}h} + e^{-3\mathrm{i}k_{\mathrm{Sz}}h}\right] \\ -k_{\mathrm{Pz}}k_{\mathrm{Sz}}\left[e^{-\mathrm{i}k_{\mathrm{Pz}}h} - 2e^{-\mathrm{i}\left(k_{\mathrm{Pz}}+2k_{\mathrm{Sz}}\right)h} + e^{-\mathrm{i}\left(k_{\mathrm{Pz}}+4k_{\mathrm{Sz}}\right)h}\right]\end{Bmatrix}$$

736 where Δ is defined as follows:

737 $$\begin{aligned}\Delta = {} & \left(k_x^2 + k_y^2 + k_{\mathrm{Pz}}k_{\mathrm{Sz}}\right)^2\left[e^{-2\mathrm{i}\left(k_{\mathrm{Pz}}+2k_{\mathrm{Sz}}\right)h} - 1\right] + 8\left(k_x^2 + k_y^2\right)k_{\mathrm{Pz}}k_{\mathrm{Sz}}\left[e^{-\mathrm{i}\left(k_{\mathrm{Pz}}+k_{\mathrm{Sz}}\right)h} - e^{-\mathrm{i}\left(k_{\mathrm{Pz}}+3k_{\mathrm{Sz}}\right)h}\right] \\ & + \left(k_x^2 + k_y^2 - k_{\mathrm{Pz}}k_{\mathrm{Sz}}\right)^2\left(e^{-2\mathrm{i}k_{\mathrm{Pz}}h} - e^{-4\mathrm{i}k_{\mathrm{Sz}}h}\right) - 2\left[\left(k_x^2 + k_y^2\right)^2 + k_{\mathrm{Pz}}^2k_{\mathrm{Sz}}^2\right]\left[e^{-2\mathrm{i}\left(k_{\mathrm{Pz}}+k_{\mathrm{Sz}}\right)h} - e^{-2\mathrm{i}k_{\mathrm{Sz}}h}\right]\end{aligned}$$

738

Appendix C

LINTRACK is a pavement tester in the Faculty of Civil Engineering and Geosciences, Delft University of Technology. As shown in Figure C1, it consists of a free-rolling wheel that moves forward and backward with a guidance system. The force applied on the wheel can be varied between 15 and 100 kN and the moving speed can be changed between 0 and 20 km/h. A fully automatic electronic control system makes it possible to run LINTRACK continuously with automatic data collection. Various measuring instruments (e.g. strain gauges) can be built into test sections to collect necessary information about the response of a pavement structure.

Figure C1. LINTRACK device with wide base tire.

References

Achenbach, J.D., 1999. Wave Propagation in Elastic Solids. Elsevier Science Publishers B.V., Amsterdam.

Al-Khoury, R., Kasbergen, C., Scarpas, A., Blaauwendraad, J., 2002. Poroelastic spectral element for wave propagation and parameter identification in multi-layer systems. Int. J. Solids Struct. 39, 4073-4091.

Al-Khoury, R., Scarpas, A., Kasbergen, C., Blaauwendraad, J., 2001. Spectral element technique for efficient parameter identification of layered media. I. Forward calculation. Int. J. Solids Struct. 38, 1605-1623.

Andersen, L., Nielsen, S.R., 2003. Boundary element analysis of the steady-state response of an elastic half-space to a moving force on its surface. Eng. Anal. Boundary Elem. 27, 23-38.

Doyle, J.F., 1997. Wave Propagation in Structures: Spectral Analysis Using Fast Discrete Fourier Transforms. Springer-Verlag, New York.

Eason, G., 1965. The stresses produced in a semi-infinite solid by a moving surface force. Int. J. Eng. Sci. 2, 581-609.

Hung, H.H., Yang, Y.B., 2001. Elastic waves in visco-elastic half-space generated by various vehicle loads. Soil Dyn. Earthquake Eng. 21, 1-17.

Jones, D.V., Le Houédec, D., Peplow, A.T., Petyt, M., 1998. Ground vibration in the vicinity of a moving harmonic rectangular load on a half-space. Eur. J. Mech. A. Solids 17, 153-166.

Lee, U., 2009. Spectral Element Method in Structural Dynamics. John Wiley & Sons, Singapore.

Lefeuve-Mesgouez, G., Le Houédec, D., Peplow, A.T., 2000. Ground vibration in the vicinity of a high-speed moving harmonic strip load. J. Sound Vib. 231, 1289-1309.

Lefeuve-Mesgouez, G., Peplow, A.T., Le Houédec, D., 2002. Surface vibration due to a sequence of high speed moving harmonic rectangular loads. Soil Dyn. Earthquake Eng. 22, 459-473.

Louhghalam, A., Akbarian, M., Ulm, F.J., 2013. Flügge's conjecture: dissipation-versus deflection-induced pavement-vehicle interactions. J. Eng. Mech. 140, 04014053.

Metrikine, A.V., 2004. Steady State response of an infinite string on a non-linear

visco-elastic foundation to moving point loads. J. Sound Vib. 272, 1033-1046.

van Dalen, K.N., Tsouvalas, A., Metrikine, A.V., Hoving, J.S., 2015. Transition radiation excited by a surface load that moves over the interface of two elastic layers. Int. J. Solids Struct. 73-74, 99-112.

Vostroukhov, A.V., Metrikine, A.V., 2003. Periodically supported beam on a visco-elastic layer as a model for dynamic analysis of a high-speed railway track. Int. J. Solids Struct. 40, 5723-5752.

Yan, K., Shi, T., You, L., Man, J., 2018. Spectral element method for dynamic response of multilayered half medium subjected to harmonic moving load. Int. J. Geomech. 18, 04018161.

You, L., Yan, K., Hu, Y., Liu, J., Ge, D., 2018. Spectral element method for dynamic response of transversely isotropic asphalt pavement under impact load. Road Mater. Pavement Des. 19, 223-238.

Zhao, M., van Dalen, K.N., Barbosa, J.M., Metrikine, A.V., 2016. Semi-analytical solution for the dynamic response of a cylindrical structure embedded in a homogeneous half-space. In International Symposium on Environmental Vibration and Transportation Geodynamics, Singapore, 369-388.

Zaghloul, S.M., White, T., 1993. Use of a three-dimensional, dynamic finite element program for analysis of flexible pavement. Transp. Res. Rec. 1388, 60-69.